Int J Earth Sci (Geol Rundsch) (2014) 103:1645–1680
DOI 10.1007/s00531-014-1021-x

ORIGInal PaPER

Near N–S paleo-extension in the western Deccan region, India: Does it link strike-slip tectonics with India–Seychelles rifting?

Achyuta Ayan Misra · Gourab Bhattacharya · Soumyajit Mukherjee · Narayan Bose

Received: 25 august 2013 / accepted: 26 March 2014 / Published online: 23 april 2014

Abstract This is the first detailed report and analyses of deformation from the W part of the Deccan large igneous province (DlIP), Maharashtra, India. This deformation, related to the India–Seychelles rifting during late Cretaceous–Early Paleocene, was studied, and the paleostress tensors were deduced. near n–S trending shear zones, lineaments, and faults were already reported without significant detail. an E–W extension was envisaged by the previous workers to explain the India–Seychelles rift at ~64 Ma. The direction of extension, however, does not match with their n–S brittle shear zones and also those faults (sub-vertical, ~nE–SW/~nW–SE, and few ~n–S) we report and emphasize in this work. Slickenside-bearing fault planes, brittle shear zones, and extension fractures in meso-scale enabled us to estimate the paleostress tensors (directions and relative magnitudes). The field study was complemented by remote sensing lineament analyses to map dykes and shear zones. Dykes emplaced along pre-existing ~n–S to ~nE–SW/~nW–SE shears/fractures. This information was used to derive regional paleostress trends. a ~nW–SE/nE–SW minimum compressive stress in the oldest Kalsubai Subgroup and a ~n–S direction for the younger lonavala, Wai, and Salsette Subgroups were deciphered. Thus, a ~nW/nE to ~n–S extension is put forward that refutes the popular view of E–W India–Seychelles extension. Paleostress analyses indicate that this is an oblique rifted margin. Field criteria suggest only ~nE–SW and ~nW–SE, with some ~n–S strike-slip faults/brittle shear zones. We refer this deformation zone as the "Western Deccan Strike-slip Zone" (WDSZ). The observed deformation was matched with offshore tectonics deciphered mainly from faults interpreted on seismic profiles and from magnetic seafloor spreading anomalies. These geophysical findings too indicate oblique rifting in this part of the W Indian passive margin. We argue that the Seychelles microcontinent separated from India only after much of the DlIP erupted. Further studies of magma-rich passive margins with respect to timing and architecture of deformation and emplacement of volcanics are required.

Keywords Deccan large igneous province · Strike-slip fault · Brittle shear · Paleostress · India–Seychelles rifting

Introduction

The K–T boundary, in the northern part of the western continental margin of India (in the states of Gujarat and Maharashtra), is marked by emplacement of voluminous flood basalts: the Deccan large igneous province (DlIP). This event relates the separation of the Seychelles microcontinent (Fig. 1) from India (Plummer and Belle 1995; Plummer et al. 1998; Subrahmanya 2001's review; Hooper et al. 2010; armitage et al. 2011; Vanderkluysen et al. 2011; Roy 2012's review). These volcanic eruptions relate the drift (implied by the Chagos–Maldive–laccadive Ridge; Fig. 1) of the Indian lithosphere over the Réunion hot spot (e.g., Morgan 1972; De 1981; Duncan 1990; Duncan and

Electronic supplementary material The online version of this article (doi:10.1007/s00531-014-1021-x) contains supplementary material, which is available to authorized users.

a. a. Misra · G. Bhattacharya · S. Mukherjee (✉) · n. Bose
Department of Earth Sciences, Indian Institute of Technology Bombay, Powai, Mumbai 400 076, Maharashtra, India
e-mail: soumyajitm@gmail.com

a. a. Misra
Petroleum Exploration, Reliance Industries limited, Reliance Corporate Park, navi Mumbai, Mumbai 400 071, Maharashtra, India

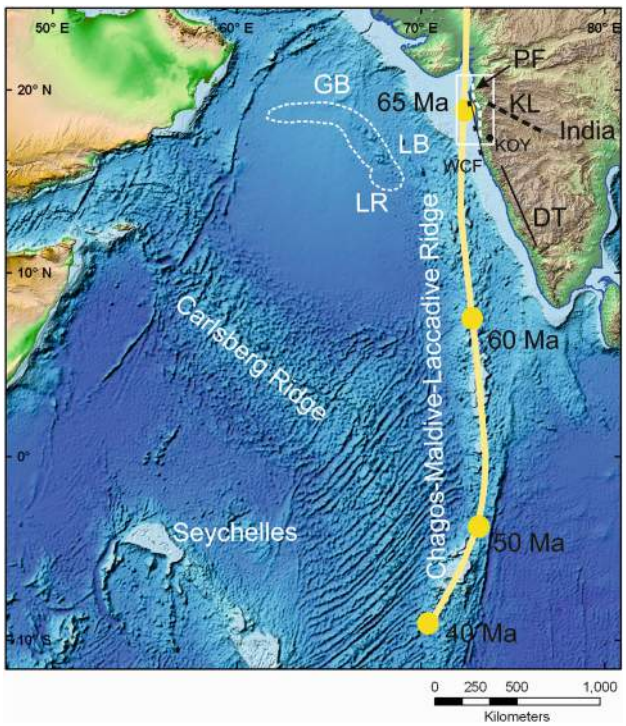

Fig. 1 Hill shaded bathymetry (*light blue* for shallower bathymetries and *dark blue* for deeper ones) and topography (*dark brown* for highest and *green* for lowest) map of a part of Indian Ocean and the arabian Sea showing the major tectonic elements. *Yellow line* track of the Rèunion hot spot (from Duncan 1990); *yellow dots* with ages: average age of the volcanics along the hot spot track (from Mahoney et al. 2002); *LR* laxmi Ridge (*white dotted outline*, approximate extent), *LB* laxmi Basin, *GB* Gop Basin, *KOY* Koyna Town, *WCF* West Coast fault, *PF* axis of the Panvel Flexure, *KL* Kurduwadi lineament, *DT* Dharwar trend, *White rectangle* area of interest for this study (Bathymetry data from Sandwell and Smith 2009; Topography data from Becker et al. 2009)

Storey 1992; Peng and Mahoney 1995; Widdowson et al. 2000; Mahoney et al. 2002; Sahu et al. 2003; Kumar et al. 2007; Sen et al. 2009; Mukhopadhyay et al. 2010; Chalapathy Rao and lehmann 2011; Ganerød et al. 2011; and van Hinsbergen et al. 2011) through impact (White and McKenzie 1989) or incubation (armitage et al. 2011). In contrast, Sheth (2005, 2007) considered plate interactions led volcanism. Seafloor spreads between India and Seychelles at ~64 Ma (Devey and Stephens 1991; Collier et al. 2008), and the Deccan traps emplaced between ~68 and 60 Ma (age estimates by lightfoot et al. 1987; Mahoney 1988; Courtillot et al. 1988, 2000; Baksi and Farrar 1991; Vandamme et al. 1991; allègre et al. 1999; Sheth et al. 2001a, b; Hofmann et al. 2000; Knight et al. 2003; Chenet et al. 2007; Hooper et al. 2010, etc.). While most of the geological publications on Deccan trap are on geochemistry (e.g., Babechuk et al. 2014), focussed structural and tectonic works are lacking till date. Duraiswami et al. (2012) considered three main tectonic zones such as narmada-Son rift, the west coast zone, and the Cambey rift, transacted the Deccan trap where fractures and dykes confine. Studying Deccan trap's fractures and faults have far reaching implications in hydrocarbon (e.g., Varun et al. 2009; azeez et al. 2011; Chandrasekhar et al. 2011; Datta Gupta et al. 2012; Pollyea et al. 2014), groundwater (such as Rai et al. 2011; review by Pawar et al. 2012; Prasanna lakshmi et al. 2014), carbon sequestration (Jayaraman 2007 and other), and geothermal energy prospects (Kumar et al. 2011).

Timing of volcanism and rifting, and eventually seafloor spreading, explains the geodynamics of "magma-rich" passive margins. Flood basalts in large igneous provinces (lIPs) may rift continents (Courtillot et al. 1999; Müller et al. 2001). Exception are Colombia River basalts, Siberian traps, Emeishan traps, and Rajmahal traps within the Kerguelen lIP. The lIPs were studied mainly on geochronology, geochemistry, and their relation with mantle plumes. High-resolution (m to km scale) structural analyses on the lIP exposures should reveal the relationship between emplacement of volcanics and breakup. Such deformation studies are relatively few in magmatic/magma-rich rifts and passive margins, e.g., Klausen and larsen (2002) for north atlantic Igneous Province in Greenland, Watkeys (2002) for Karoo volcanics in SE africa, and Miggins et al. (2002) for Rio Grande rift in south-central Colorado and northern new Mexico.

Few studies (Table 1 of Menzies et al. 2002 and references) revealed that volcanics in lIPs can be pre-, syn-, or post-rift. White and McKenzie (1995) concluded that the peak volcanic activity *"shortly predates"* the oldest seafloor spreading anomaly. In the specific case of microcontinent Formation, as in ours, magmatism presumably predated and triggered rifting (Müller et al. 2001). However, recent geophysical studies on India–Seychelles conjugate margins concluded magmatism to postdate the main rifting. This questioned how pluming formed microcontinents (Calvès et al. 2008; Collier et al. 2009). In passive margins, magmatism postdates rifting (Péron-Pinvidic and Manatschal 2010) after substantial crustal thinning. In contrary, Richards et al. (1989) suggested that rifting postdated volcanism in lIPs and does not require a precursor thinned lithosphere.

The volcanic rocks of the Kalsubai, lonavala, and lowermost Wai Subgroups (see "Regional geology" section and Table 1 for stratigraphy; Deshpande 1998; Table 1 of Duraiswami et al. 2012; Parthasarathy et al. 2013; see Schöbel et al. 2014 for magneto-stratigraphy) in the western DlIP) underwent maximum crustal contamination among the entire Deccan volcanic terrain (Cox and Hawkesworth 1984; Devey and lightfoot 1986; Ray et al. 2014). This proves that significant crustal thinning did not happen by then (Saunders et al. 2007). Thus, a major rifting phase was either coeval or postdated volcanism. The

Table 1 Stratigraphy of the Deccan large Igneous Province (after Beane et al. 1986; Mitchell and Widdowson 1991; Godbole et al. 1996; Widdowson et al. 2000; and Vaidhyanadhan and Ramakrishnan 2008; lithologies from District Resource Maps of Mumbai, Thane, Raigad, Ratnagiri, Pune districts, Geological Survey of India 2001). See Fig. 2 for occurrence of Formations.

Subgroups	Formations		Dominant lithology
	lithostratigraphy	Chemostratigraphy	
Salsette	Borivali	Mumbai volcanics	Trachytes, rhyolites, tuff, agglomerates, intertrappeans, etc.
Wai	Mahabaleshwar	Desur Panhala Mahabaleshwar	Fine to medium-grained, moderate to sparsely porphyritic flows
	Purandargarh	ambenali	
	Diveghat	Poladpur	
	Elephanta		
lonavala	Karla	Bushe	
	Indrayani	Khandala	Fine to medium-grained aphyric flows
Kalsubai	Ratangarh	Bhimashankar	Dense aphyric to phyric flows with moderately porphyritic pahoehoe flows
	Salher	Thakurwadi	
		neral	
		Igatpuri	
		Jawhar	

India–Seychelles breakup indicated by organized seafloor spreading at ~63.4 Ma (Collier et al. 2008) *postdated* the peak volcanism (~65 Ma). a slightly older age of breakup (65 Ma), coinciding with the Deccan basalt eruption, has also been suggested (Table 3 of Bastia et al. 2010; also see Reeves 2013a, b). That would indicate that the rifting was *coeval* to volcanism. notice that a controversy exists whether volcanism leads to rifting or vice versa (Fowler 2005).

Fieldworks and geochronologic studies from the Indian W coast margin (India–Seychelles conjugate margin) revealed that most of the volume (> 80 %: Chenet et al. 2007) of the exposed ~68–60 Ma Deccan traps emplaced before rifting initiated (Devey and Stephens 1991; Saunders et al. 2007; Hooper et al. 2010; Ganerød 2010; Ganerød et al. 2011). Deformation in the Deccan traps exposed along the n part of the W coast of India should therefore reflect the tectonics of the India–Seychelles rifting, which ended with their breakup at ~63.4 Ma (Devey and Stephens 1991; Collier et al. 2008).

as per current understanding, a ~E–W extensional tectonics, deciphered plausibly from n–S-trending dykes, coeval to late phases of Deccan volcanisms explains the India–Seychelles rifting (Hooper 1990; Bhattacharya et al. 1994; Hooper et al. 2010; Vanderkluysen et al. 2011). Three sets of sub-vertical fracture planes were deciphered from Powai, Mumbai, and two of them (nW and nE trending) were considered to be conjugate to decipher an approximate n–S extension (Sen 2011). Dessai and Bertrand (1995) and Hooper et al. (2010) reported ~n–S (brittle) shear zones from coastal areas of Deccan. However, they did not resolve stresses that deformed these rocks. Interestingly, ~n–S vertical strike-slip shear zones cannot result from a ~E–W extension. Ju et al. (2013) deciphered ~E–W paleostress fields from the DlIP based solely on ~n–S trends of mafic dyke swarms mapped by others (viz. Beane et al. 1986; Sheth 2000; Vanderkluysen et al. 2011). Recently, some evidences of compression by W verging thrusts (Kaplay et al. 2013) were deciphered near nanded city, which is ~400 km E from the coast. Tectonic significance with respect to the passive margin Formation is difficult to ascertain from Kaplay et al. (2013). The reasons are (1) though a "recent" age has been indicated, no particular age has been confirmed for the event; and (2) it is far off from the continental margin and with a large area in between with no faults/dykes reported.

a detail study on the deformation structures seemed necessary to explore the tectonics of the coastal Deccan basalts (Fig. 2) around Mumbai (formerly known as "Bombay"). We deduced and examined the "apparent" mismatch between the trend of the shear zones and direction of extension. We analyzed paleostresses from field and remote sensing studies. We covered ~150 km along ~n–S and ~100 km along ~E–W in the field and a larger area in remote sensing. Only the brittle deformation structures were studied since (semi-) ductile structures were absent.

Sub-vertical brittle shear zones/faults trend ~nW–SE or ~nE–SW and some ~n–S. The paleostress analyses yielded a wide range from nW to nE-trending extension in the terrain. This contradicts the present ~E–W extension. This would be a crucial input for the tectonics of the west coast of India because a near n–S extension implies

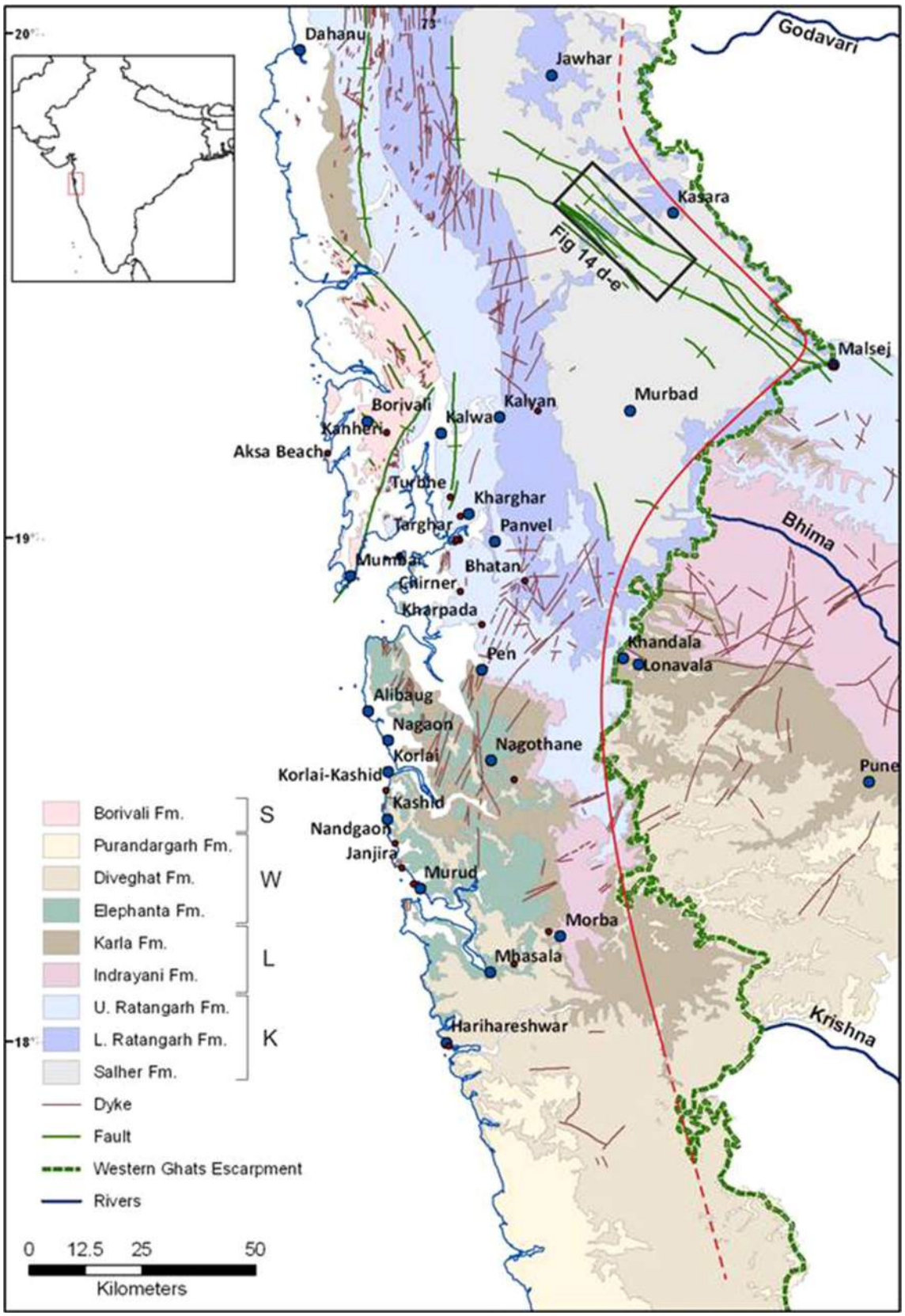
Dahanu
Jawhar
Godavari
Kasara
Fig 14 d-e
Malsej
Murbad
Kalyan
Kalwa
Borivali
Kanheri
Aksa Beach
Turbhe
Kharghar
Targhar
Panvel
Bhima
Mumbai
Bhatan
Chirner
Kharpada
Pen
Khandala
Lonavala
Alibaug
Nagaon
Korlai
Nagothane
Pune
Korlai-Kashid
Kashid
Nandgaon
Janjira
Murud
Morba
Mhasala
Harihareshwar
Krishna
20°
19°
18°
73°
Borivali Fm.
Purandargarh Fm.
Diveghat Fm.
Elephanta Fm.
Karla Fm.
Indrayani Fm.
U. Ratangarh Fm.
L. Ratangarh Fm.
Salher Fm.
S
W
L
K
Dyke
Fault
Western Ghats Escarpment
Rivers
0 12.5 25 50
Kilometers

◀**Fig. 2** Study area showing the Formations ("Fm") of the Deccan volcanic province (coastal region). Salher Fm is the oldest while Borivali Fm is the youngest. Younger Formations are encountered towards south.*Brown lines* dykes; *blue lines* faults as per Geological Survey of India (District Resource Maps 2001); *blue large dots* sizeable settlements; *red smaller dots* field locations; *red solid line* western Deccan strike-slip zone mapped. The n and S limits await mapping and hence marked as *dotted red lines*. Blank areas (in *white*): either limits of district boundaries or water bodies or alluvial cover. *Green line* Western Ghats escarpment (Widdowson and Cox 1999). *Black rectangle* at nE: location of Fig. 14d, e; K: Kalsubai Subgroup; l: lonavala Subgroup; W: Wai Subgroup; S: Salsette Subgroup. *Inset* map indicates the extent (in *red rectangle*) of the area around Indian west coast

that the margin is a "sheared margin" or an "oblique rifted" margin. On the other hand, an E–W extension would indicate an orthogonal extension.

Studying different aspects of this exposed magma-rich sheared passive margin, supposedly its proximal part would reveal relationships between the lIPs and the rift-related processes. This could explain various microcontinent Formation processes.

Regional geology

Stratigraphy

The DlIP is well studied lithostratigraphically (Table 1; Godbole et al. 1996; Vaidyanadhan and Ramakrishnan 2008) and chemostratigraphically (Beane et al. 1986; Mitchell and Widdowson 1991; Widdowson et al. 2000; Peng et al. 2014 and others). In these schemes, "Formations" differ, yet the Subgroups remain the same (Vaidhyanadhan and Ramakrishnan 2008; Table 1 for comparison). From n to S, Kalsubai, lonavala, and Wai Subgroups comprising mainly basaltic flows of various thicknesses show progressive younging (Fig. 2; Devey and lightfoot 1986; Beane et al. 1986; Widdowson et al. 2000). Compound flows occur in western part of Deccan trap, whereas simple flows in other areas (fig. 1 of Duraiswami et al. 2012). The Salsette Subgroup volcanics (Borivali Formation or Salsette Island volcanics or Mumbai volcanics) is acidic. It consists of minor intrusives and intertrappean sediments (Cripps et al. 2005) restricted within the Mumbai region (Fig. 2). The DlIP emplaced possibly in pulses (Chenet et al. 2007) during ~68–60 Ma. This contradicts emplacement in a shorter duration (e.g., Courtillot et al. 1986; Duncan 1990) around the K/T boundary.

Dykes

The dykes in the DlIP are of three regional groups of similar lithologies viz. gabbro, dolerite, lamprophyres, and nepheline syenite. (e.g., Dessai and Bodas 1984; Ray et al. 2007, 2008; Hooper et al. 2010). These are (1) the linear EnE–WnW narmada–Satpura–Tapti feeder dyke system; (2) the ~n–S West Coast dyke swarm; and (3) the nnE–SSW weakly oriented nasik–Pune swarm (Deshmukh and Sehgal 1988; Bondre et al. 2006; Ray et al. 2007; Valdiya 2011; also see Powar 1981; Duraiswami et al. 2012). Geochemical and some geological descriptions of dyke systems are available in Beane et al. (1986), Dessai and Viegas (1995), Sheth (2000), Vanderkluysen et al. (2004), Jain and Gupta (2013), etc. Only the EnE–WSW dykes are present in the study area. Detailed study of the lineaments, which are mostly dykes (see "Remote sensing analyses" section, this work) reveal that the coastal swarm also widely vary in trend (Fig. 2). Dykes are absent eastwards from 75°E (Deshmukh and Sehgal 1988) and reappear in the narmada region.

an estimated average extension ratio expressed in % (see Ju et al. 2013 for details) deciphered from the dykes yielded values ~30 % (Dessai and Bertrand 1995), 18 % (Bhattacharji et al. 1996), ~5 % specifically from Rajpipla sector (Valdiya 2010), and ~4–5 % in different areas (Ju et al. 2013).

Hooper et al. (2010) identified three sets of dykes geochemically and geochronologically from Mumbai and nearby regions. Their ages are 66–65, ~65, and 65–63 Ma. They reported two of these sets to be strongly ~n–S oriented regionally, i.e., parallel to the ~n–S shear zones, but some cut across shear zones locally. The third group has reportedly weak orientation and predates the shear zones. Hooper et al. (2010) concluded that (1) deformation took place after the bulk of the Deccan traps existed; (2) rift-related structures developed by 65–64 Ma; and (3) the Salsette Subgroup erupted during the break up and attenuation of the western continental margin.

Tectonics

although Plummer and Belle (1995) and Ganerød et al. (2011) considered that a plume rifted India from Seychelles, it may also be due to far-field stresses leading to extensional tectonics in the West Indian passive margin (Malod et al. 1997; Courtillot et al. 1999; review by Mahadevan 1994; Balasubrahmanyan 2006; Hooper et al. 2010; Vanderkluysen et al. 2011). Seychelles rifted from India after the lowermost Formations of the Wai Subgroup (Table 1; Fig. 1) emplaced (Hooper 1990; Hooper et al. 2010). Hooper et al. (2010) concluded that the main volcanism predated rift-related extension. The bulk volcanism completed before ~66–65 Ma, and Seychelles broke away from India by the start of the magnetic chron C28n–C27n (64–63 Ma) (Todal and Edholm 1998; Collier et al. 2008; Ganerød 2010; Ganerød et al. 2011). This proves that the rifting happened after the bulk of the Deccan basalts

emplaced within 68–65 Ma. Dykes and other alkaline felsic rocks from Seychelles Islands of ages 63.5–61 Ma (Ganerød et al. 2011) resemble geochemically the dykes and other volcanics in and around Mumbai (Hargraves and Duncan 1990; Devey and Stephens 1991, 1992; Ganerød et al. 2011; Owen-Smith et al. 2013). Owen-Smith et al. (2013) conclude that the Seychelles alkaline felsic suite represents the peak Deccan volcanism and start of the India–Seychelles rifting. These evidences point that breakup postdated the major/bulk Deccan volcanism. again, lagoonal to shallow marine intertrappeans (Cripps et al. 2005) confined within the Borivali Subgroup (~63–60 Ma) implies marine influence to begin by this age. From this constrain on the age of the Deccan basalts, and the timing of India–Seychelles breakup, Deccan rocks should reveal deformation related to rifting.

The Panvel flexure (Fig. 1) is a regional monocline (auden 1949) dipping W to ~2–15° and formed at 65–64 Ma (Hooper et al. 2010) or 63–62 Ma and thereafter (Sheth and Pande 2014) by rifting India from Seychelles. Increase in dips of the volcanic flows toward the arabian Sea defines it (see Dessai and Bertrand 1995; Sheth 1998). Dykes define the extent and the trend of this flexure (Dessai and Bertrand 1995). The area presently shows microseismicity from shallow to deep (~2–15 km) levels (Mohan et al. 2007; also see Guha and Padale 1981; Mishra 2012a, b; Rai and Ramesh 2012). Mahadevan (1994) reviewed Deccan crustal structure. The Panvel flexure was explained as either a rift-related primary flexure (Devey and lightfoot 1986) or a flexural response of the Western Ghats uplift and associated offshore subsidence (Watts and Cox 1989). The Panvel flexure was described as a syn- or post-rift extensional fault structure comprising of tilted fault blocks (Dessai and Bertrand 1995; Dessai and Viegas 1995). Sheth (1998) explained it as a reverse drag (Mukherjee 2013a) on a large listric fault in the Mumbai offshore. However, seismic data in Mumbai offshore did not reveal such fault (Verma et al. 2001; naik et al. 2006; Misra et al. 2013). The flexure, thus, awaits a tectonic explanation, but we do not address this.

Steep mesas in and around Mumbai under a tropical climate possibly indicates the role of some hitherto undiscovered structures from the Deccan trap (Bhattacharya 2013). The ~nW–SE trending, ~500 km long Kurduwadi/Kurudwadi lineament, has been previously envisaged, from gravity anomalies, to be a subtrappean rift (Brahmam and negi 1973; also see Qureshy 1981; Mishra et al. 2008; Mishra 2012a, b). alternately, from geomorphological studies and from satellite and areal imagery, Peshwa and Kale (1997) interpreted the Kurduwadi lineament to be a deep crustal-scale shear zone in the sub-trappean Precambrian rocks comprising of several ~nW–SE dextral faults. The Kurduwadi lineament correlates the dextral ~nW–SE Wadi fault in the neo-proterozoic Bhima basin and in the archean Dhawar granite gneisses (Kale and Peshwa 1995; Peshwa and Kale 1997). This lineament has also been confirmed as a sub-trappean fault zone from magnetotelluric studies (Harinarayana et al. 2007). The Kurduwadi lineament depicts deformation in the Quaternary sediments in its northernmost part near Sangamner (Dole et al. 2000) and southernmost part in the Terna River basin (Babar et al. 2012). Few authors (Dole et al. 2000; Babar et al. 2012) considered the deformation by reactivation of the faults, and seismicity by differential compaction and loading of the Deccan volcanics. The ~nnW West Coast fault (Chandrasekharam 1985; Biswas 1987) and the nnE-trending Koyna fault (Sarma et al. 2004) are two important fault zones that might have played key role in the tectonics of the western continental margin of India. The West Coast fault was possibly passive during Triassic–Jurassic and reactivated in Cretaceous–Early Paleocene (Biswas 1987), whereas the Koyna fault depicts recent activity as understood from geophysical studies (Kaila et al. 1981; Sarma et al. 2004). a nnE-trending strike-slip fault zone dipping ~60° toward WnW has also been confirmed near Koyna dam from drilling (Gupta et al. 1999) and geophysical studies (Sarma et al. 2004 and references therein). The sense of slip of the Koyna fault is not confirmed till date. Both the West Coast fault and the Koyna fault follow the Dharwar foliation trend (see fig. 2 of Gombos et al. 1995) (Fig. 1). Geophysical and remote sensing studies (Harinarayana et al. 2007; Chandrasekhar et al. 2011; Kumar et al. 2011) identified faults in the Deccan traps. The faults are concentrated in the rifted zones, viz., narmada rift zone, Cambay rift, and West Coast passive margin. Those faults are steep and trend variedly from nE to nW. Sense of slip, dips of fault planes, and other such details of these faults are not available.

Kolla and Coumes (1990) reviewed and compared the structural trends in the onshore and offshore continental sectors along the Indian western continental margin. While across major parts of the DlIP, the volcanic flows are horizontal, they dip variably around the Mumbai coastal area. Their westerly dips steepened during Tertiary due to subsidence by crustal thinning and sediment loading at the passive margin (Sheth 1998; Chaubey et al. 2002; Mohan and Kumar 2004; Cripps et al. 2005).

a number of researchers investigated the magnetic seafloor spreading anomalies in the n arabian Sea (e.g., Bhattacharya et al. 1994; Dyment 1998; Miles et al. 1998; Todal and Edholm 1998; Collier et al. 2008; Misra et al. 2013). "Discussion and conclusions" section summarizes the results of their mapping, n and S of the laxmi ridge, and the magnetic anomalies trend ~E–W. Magnetic anomalies between the laxmi ridge and the Indian continent trend ~nnW–SSE (Bhattacharya et al. 1994; Talwani and Reif

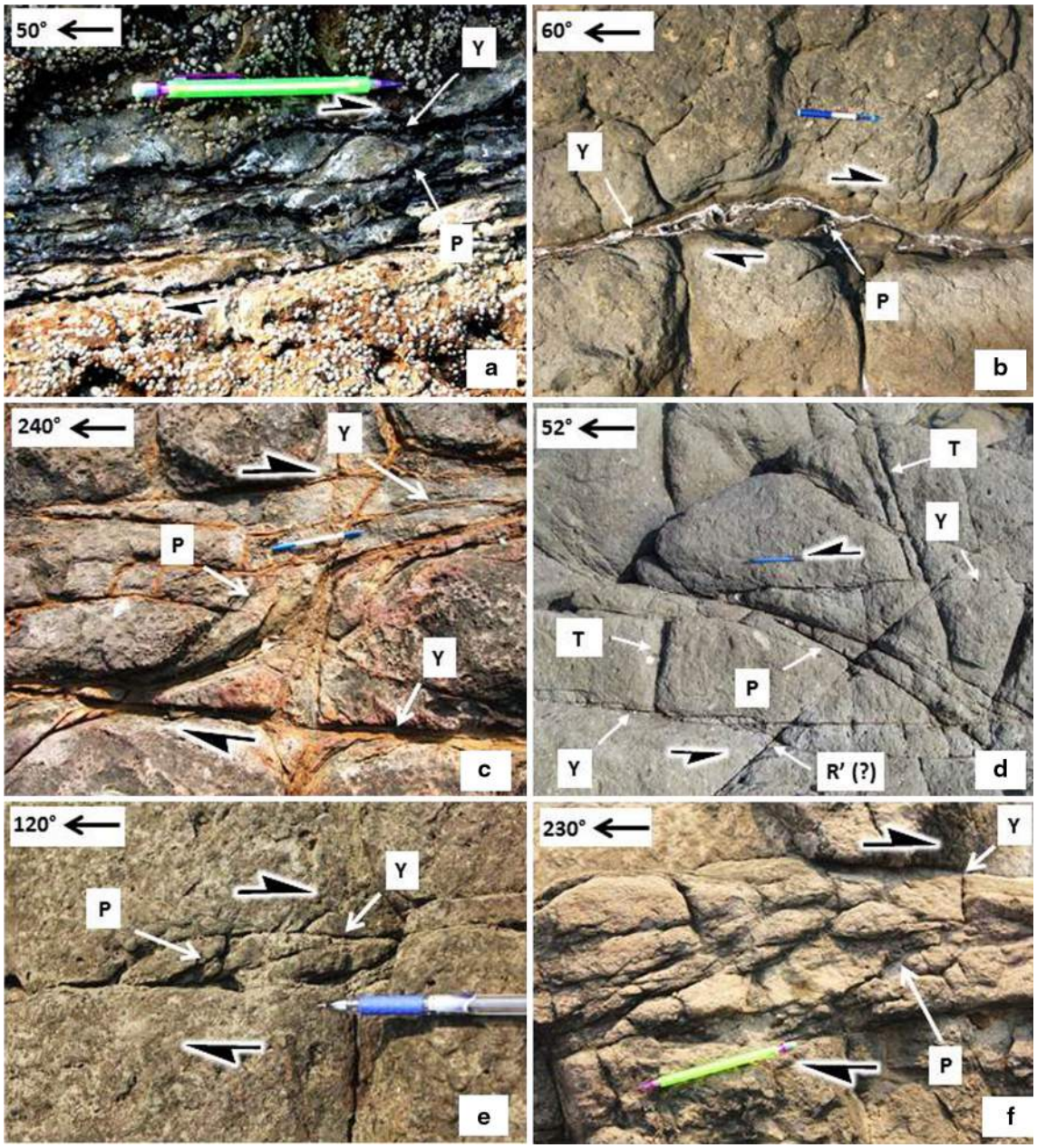

Fig. 3 Outcrops of brittle shears on sub-horizontal exposures with prominent *P*- and *Y*-planes, **a** sub-vertical strike-slip brittle shear, with close-spaced *Y*- and sigmoid *P*-planes, define a strike-slip brittle shear (nandgaon Beach, loc: 18°23′34.37″n, 72°55′14.47″E); **b** curved *Y*-plane and *P*-planes define a brittle shear. Mineralized shear planes at Janjira (loc: 18°20′51.78″n, 72°55′8.54″E); **c** sub-vertical brittle shears with evident *P*- and *Y*-planes at aksa Beach (loc: 19°10′2.83″n, 72°46′53.49″E); **d** conspicuous *P*-, *Y*-, *T*-planes on outcrop, with a possible *R*′ shear associated with a sinistral brittle shear at Korlai–Kashid (loc: 18°29′16.02″n, 72°54′1.23″E); **e** small unambiguous brittle shear at Murud (loc: 18°18′42.84″n, 72°57′32.80″E); **f** intricate network of close-spaced sigmoidal *P*-planes by planar *Y*-planes at Harihareshwar (loc: 17°59′21.23″n, 73° 1′37.24″E). Refer Fig. 2 for locations

1998) or ~nW–SE (Todal and Edholm 1998). Yatheesh et al. (2009) demonstrated a mismatch between the magnetic anomalies in this region and the "typical" anomaly patterns. They also cautioned that the same magnetic data can interpret multiple ages (their fig. 8). Calvès et al. (2011) too supported this in their fig. 2.

Structural geology

Brittle shears and striated fault planes

We studied sub-horizontal and sub-vertical outcrops in field at rocky beaches, road cut sections, quarries, river

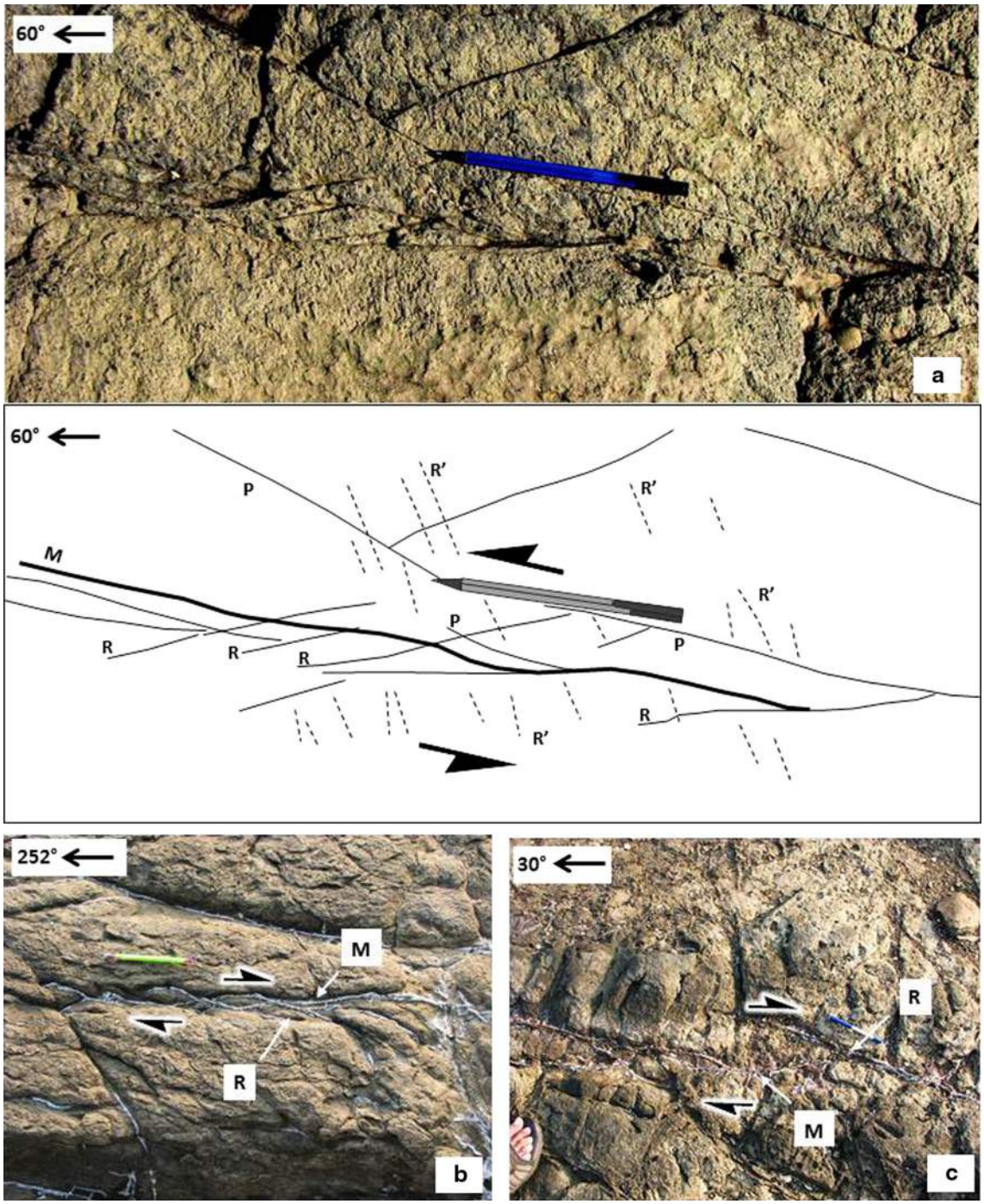

Fig. 4 Outcrops of Riedel shears on sub-horizontal exposures, **a** *R* shears (*top*), with line drawing (*below*), at Korlai–Kashid rocky beach, north of Kashid beach. *R*- and *P*-planes are marked by *solid lines*. Incipient *R*′ fractures marked by *broken lines* and the "average slip plane" (*M* shear) by a *bold black line* (loc: 18°29′58.52″n 72°54′13.89″E); **b** sub-vertical dextral Riedel shears with mineralized (zeolite) *M*- and *R*-planes at nandgaon (loc: 18°23′34.37″n, 72°55′14.47″E); **c** mineralized *M*- and *R*-planes dextral sheared at Janjira (loc: 18°20′51.78″n, 72°55′8.54″E). Refer Fig. 2 for locations

terraces, etc., in and around Mumbai (Fig. 2 for field locations). Brittle shears were documented from all the four Subgroups (stratigraphy in Table 1). We documented brittle shears, slickensided fault planes, steps, asymmetric elevations (Doblas 1998), slipped markers, Riedel shears (Petit 1987; Passchier and Trouw 2005; Fossen 2010), etc. We define this zone of brittle deformation along the west coast India as the "Western Deccan Strike-slip Zone" (or

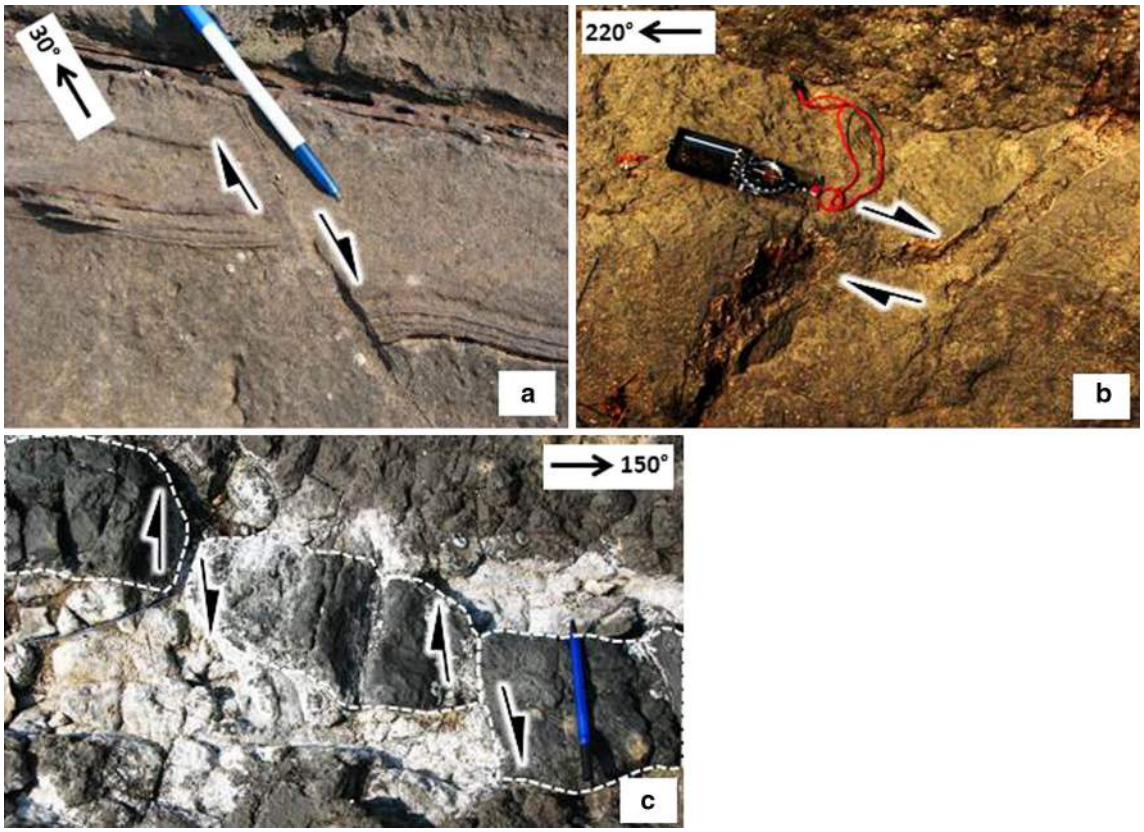

Fig. 5 Examples of slipped markers on sub-horizontal outcrop **a** mineralized fractures slipped dextrally at aksa Beach (loc: 19°10′2.83″n, 72°46′53.49″E); **b** slipped vein along a fault plane at Kharghar hills (loc: 19°02′28.21″ n, 73°03′05.21″E); **c** displacement of a dyke along shears, at Murud (loc: 18°18′42.84″n, 72°57′32.80″E). The group of dykes deformed by the shears forms the Group I dykes of Hooper et al. (2010), which predate the deformation. Refer Fig. 2 for locations

WDSZ). Figure 2 shows the possible extent of the WDSZ. It extends from the Western Ghats escarpment (Fig. 1) to the coast. The n-S extent of the WDSZ needs delineation.

The sub-vertical *Y*-planes (see p. 157 of Passchier and Trouw 2005 for brittle shear nomenclatures) trend ~nW–SE/~nE–SW (with some ~n–S) in the older lower and Upper Ratangarh Formations and ~nW–SE/~nE–SW (with minor ~nnE-SSW) in the younger Elephanta, Karla, and Borivali Formations. The *P*-planes of the brittle shears, bound within the *Y*-planes, are sigmoid. In other words, the *Y*-planes are tangential to the *P*-planes. The shear sense is deciphered from the angular relationship between the *Y*- and the *P*-planes (see Passchier and Trouw 2005 for details; Mukherjee 2007, 2010a, b, 2012c, 2013b, c, d; Mukherjee and Koyi 2010a, b), similar to *C*- and *S*-planes for ductile shears (Berthé et al. 1979; Mukherjee 2011; Chen et al. 2014). The angles between the *Y*- and the *P*-planes range 25–45° (Passchier and Trouw 2005; Fossen 2010; Davis et al. 2012), and our estimated angles (~30–40°) fall within this. *Y*-planes, same as the "fault planes" (Davis et al. 2012). In some exposures, sub-vertical ~nE to ~EnE-trending Riedel shears (Figs. 3d, 4a) associate with the brittle shears. Since sub-vertical (> 80°) *R*-, *R*′-, and *M*-planes (Petit 1987; Passchier and Trouw 2005) were found on sub-horizontal outcrops, they denote a strike-slip deformation. Markers such as mineralized fractures at aksa Beach (Fig. 5a), veins at Kharghar hills (Fig. 5b), and dykes near Murud (Fig. 5c) slipped dextrally along ~nnE–SSW to ~nE–SW sub-vertical, strike-slip faults. Strike-slip brittle shears (Fig. 3a–f) are prominent at aksa Beach, Kashid-Murud stretch, and nagothane–Harihareshwar locations (Fig. 2 for field locations) with dominantly dextral shear. Secondary mineralizations (Figs. 3b, 4a, b) seen often along brittle/Riedel shears (*R*- and *R*′-planes), made the shear sense indicators more conspicuous. *R*-planes have a typical angle of 10–20° and the *R*′-planes 70–110° with the *M*-planes (Petit 1987; Passchier and Trouw 2005; Fossen 2010). In our case, the angle between the *R*- and the *M*-plane is 10°–15° and that between the R′- and the *M*-plane 70°–90°. Sinistral brittle shears were rare (Figs. 3d and 4a). However, a km-scale regional sinistral shear, what we designate as the "Jawhar–Malshej shear zone," is evident in the satellite images ("Data and methods" section). Shear fractures crosscut (Fig. 6) at nagothane and near

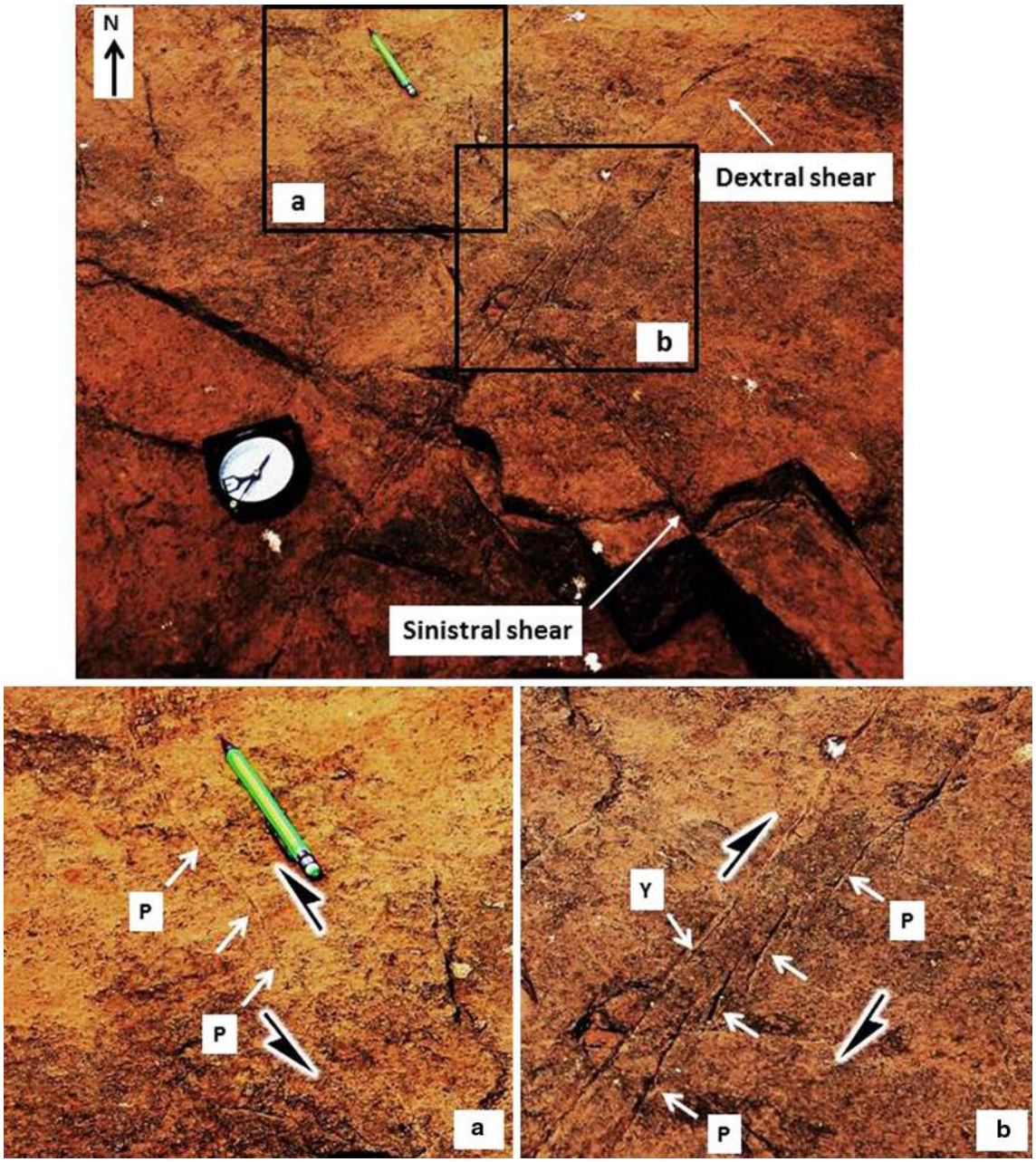

Fig. 6 Crosscutting shear fractures on sub-horizontal outcrops near Mhasala (loc: 18°09′14.06″n, 73°09′27.64″ E). The shear fractures trending nW–SE (*left side* in photograph) are sinistral, whereas those trending nE–SW (*right side* in photograph) are dextral. **a** and **b** zooms into parts (marked by respective *labeled boxes*) of the main photograph (*above*) to show the details of the shears. *White arrows* mark the *P*-planes. Sinistral shear not well-formed, refer Fig. 2 for locations

Mhasala (Fig. 2 for field locations) with sinistral ~330°n trending shears (= *Y*-plane) and dextral ~20°n trending shear. Both the crosscutting shears accompany sub-vertical *P*-planes making ~10–20° angles with the *Y*-planes. Since these crosscutting shears are not compatible with the σ_1 (maximum compressive stress) bisector of the small angle of the crosscutting pair, which is typical of "conjugate shear fractures" (Fossen 2010), we considered both the brittle shear planes as independent data points for the stress analyses in "Paleostress analyses" section.Whether the strike slip brittle sheared rock under optical microscope reveal trapezoid-shaped minerals (as in Mukherjee 2012a, b) is a subject of future study.

Riedel shears (Petit 1987) are common in strike-slip domains but were reported subsequently from other shear zones (Davis et al. 1999; Katz et al. 2004). The Riedel

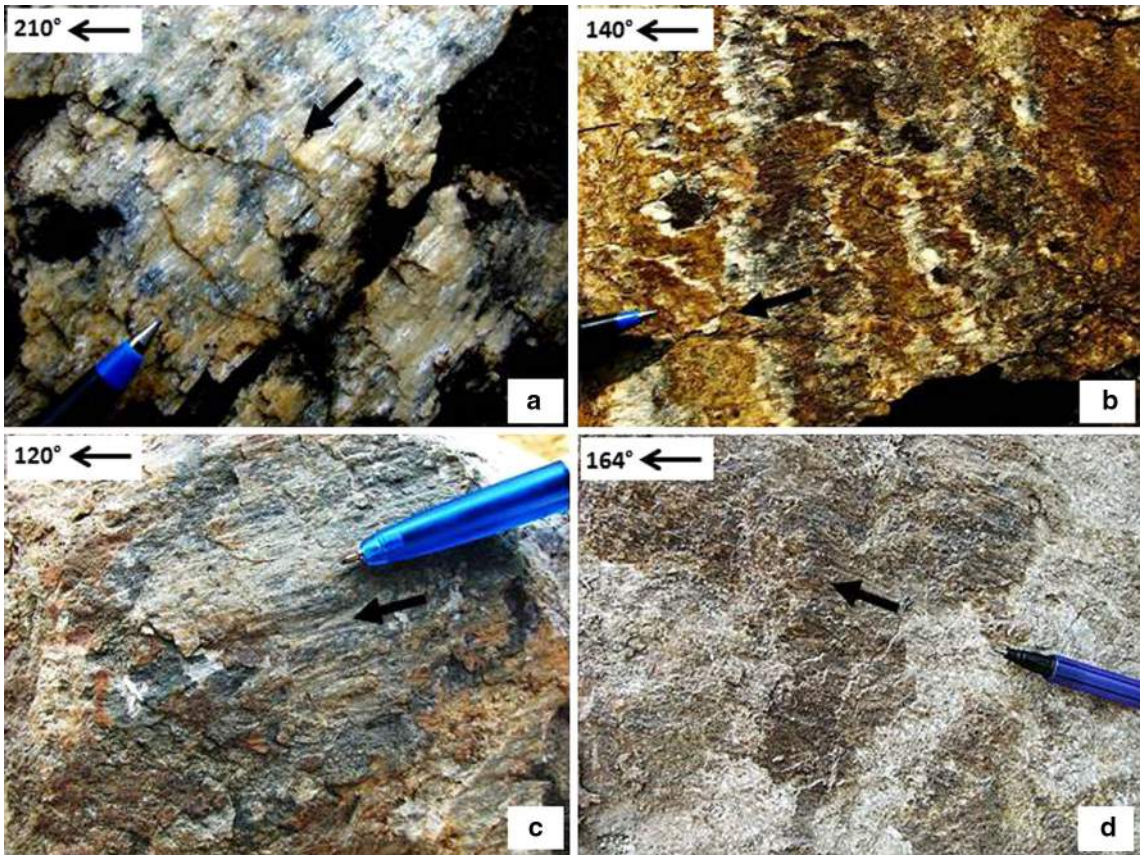

Fig. 7 Polished slickensided fault planes (sub-vertical) represent a dextral oblique-slip movement on sub-vertical fault plane at **a**, **b** Kharghar hills (loc: 19°02′28.21″n, 73°03′05.21″E); **c** Turbhe (loc: 19°4′55.43″n, 73° 1′53.31″E): **d** Varcha–Owle (loc: 18°59′28.02″n, 73°2′28.29″E). The striae pitch 10–15° on the fault plane in these examples contrasts (**a**), which is ~50°. *Bold black arrows*: movement direction of the missing block. Refer Fig. 2 for locations

shear zones can show the secondary R and R' shears (or R_1 and R_2, respectively, as per Ramsay and Huber 1987) and T- (T = tensile) fractures/planes with the "average" or "mean" or "main" slip plane (M-plane) (Petit 1987). This M-plane is not to be confused with "movement plane" (see Fossen 2010). The "movement plane" is an imaginary plane required for the construction of "tangent-lineation diagrams" for fault populations (Fossen 2010). We denote "M-plane" here as the main slip plane. If Riedel and non-Riedel brittle shears coexist, the M- and the Y-planes coincide. In this case, the M-plane is equivalent to the Y-plane. The R shears develop first (Ramsay and Huber 1987) in strike-slip regimes and are thus more abundant. The main movement occurs along the M-plane (thus = fault plane) and so often they bear slickensides (Petit 1987). The shear sense is deciphered from the slickensides and/or the angular relationship between the R/R' shears with the M-plane. We noticed Riedel shears (R and R'), occurring along with Y–P planes, T-fractures, and ~nE–SW trending M-planes on sub-horizontal outcrops at nandgaon and Korlai–Kashid (Fig. 4; Fig. 2 for field locations). R and R' shear planes occur at ~10–20° and ~70–90°, respectively, with the Y-planes.

Slickensides on striated fault planes (Fig. 7; see fig. 1 of Doblas 1998's review) were observed in the quarries and road cut sections at Kharpada, Panvel, Kharghar, Varcha-Owle, and Murbad (Fig. 2: field locations). In general, they occur on freshly exposed, thin (~1–5 mm), mineralized (secondary quartz, zeolite, calcite, etc.) fault planes and show dominantly a dextral slip. Mineralized films are prone to erosion (Whiteside 1986; Doblas et al. 1997; Doblas 1998; Kranis 2007). This might be the cause of their absence in large parts of the WDSZ. The nW to nE (minor ~n–S to ~nnE–SSW) trends of the striated faults planes match those of the Y-planes of the brittle shears. Pitch of slickenlines on sub-vertical faults range widely from 0 to 90°. Thus, those are strike-slip, oblique-slip, and dip-slip faults. notice that although Tjia (1964) questioned reliability of slickenslides to determine brittle shear sense, subsequent workers used slickensides to decipher shear sense.

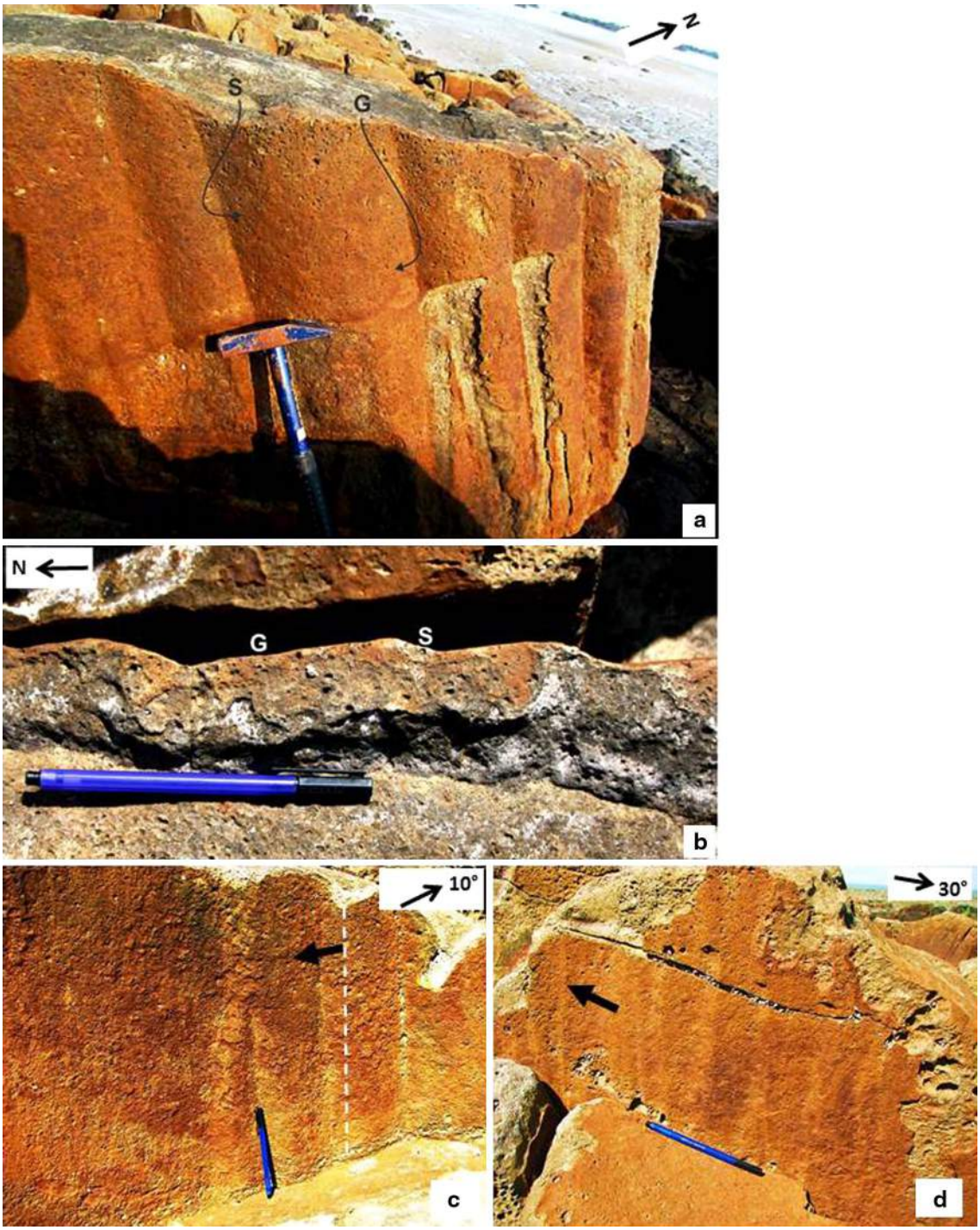

Fig. 8 **a** On a sub-vertical section, a train of "asymmetric elevations" or knobby elevations (of Doblas 1998) indicate a dextral strike-slip fault, "g" indicates the gentle slope; and "s" its steep slope. note the plucking on the steep slopes resemble roche moutonnées; **b** Transverse section of "asymmetric elevations" also indicate a dextral slip, "g" and "s" have same meaning as in **a**, (modified from Misra and Bhattacharya 2014); **c** another train of asymmetric elevations. note the branching morphology (near the pen). The general trends of the elevations are used to measure the slip vector. The slip vector is measured perpendicular to the crest of the elevation, marked by the *white dotted line*; **d** another example of an asymmetric elevation, but with a smoother surface; at aksa Beach (loc: 19°10′10.88″n, 72°47′21.44″E), refer Fig. 2 for locations

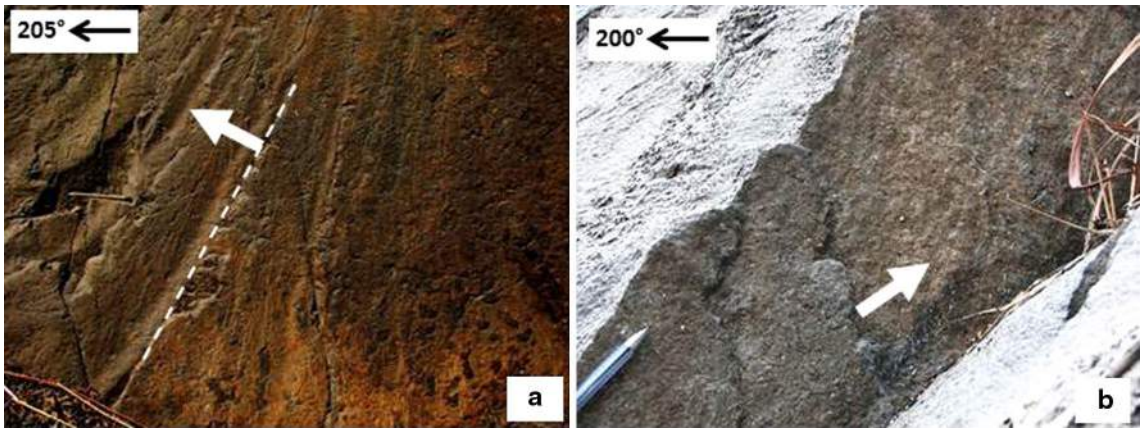

Fig. 9 Slickenside-bearing fault planes (sub-vertical) with steps, **a** dextral strike-slip fault plane (near Kharpada bridge, loc: 18°49′36.11″n, 73°05′36.57″E); **b** steps on a sinistral fault plane, at a quarry near Murbad (loc: 19°15′2.55″n, 73°12′23.87″E), *white arrows* sense of movement of missing block, refer Fig. 2 for locations

asymmetric elevations/knobby elevations (Dzulynski and Kotlarczyk 1965; Tjia 1967)/"steps" (Doblas 1998), a kind of rare slickensides, were documented as reliable shear sense indicators (type aE-3 in Fig. 1 of Doblas 1998; Misra and Bhattacharya 2014). Slopes of their steep faces indicate the shear sense of the missing block. Parts of their steep slopes plucked off (Dzulynski and Kotlarczyk 1965; Tjia 1967; Misra and Bhattacharya 2014; Fig. 8). Those are abundant on ~n to nE-trending sub-vertical faults at aksa Beach (Fig. 2: field location) and denote dextral shear. although geometrically similar, these should not be confused with mullions. Mullions develop at lithology interfaces with significant competence contrast (Davis et al. 2012; see also Misra and Bhattacharya 2014). Here, asymmetric elevations develop solely in rhyolites and their positive smoothness criterion ("good" degree of confidence; Doblas 1998) reveals shear sense. Steps (Doblas 1998) occur on polished fault planes as isolated structures (Fig. 9). Polished fault planes are smooth when rubbed gently along the slip of the missing block. These planes feel rough when rubbed oppositely. These are sometimes associated with asymmetric elevations. Steps are rarer than striated fault planes.

near n–S (with some ~nW/nE), vertical dip-slip faults/brittle shears were fairly common. Dessai and Bertrand (1995) and Valdiya (2011) also reported/referred n–S trending vertical dip-slip faults from this area. Sub-vertical faults neither extend nor compress the crust. andersonian dip-slip fault dip < 60° (anderson 1951), which is not the case here. Vertical dip-slip faults imply only vertical movements of the crust (Maldonaldo and Stanley 1976; Waldron et al. 2007). Isostatic loading by sedimentation, volcanism, glaciation, etc., or unloading by erosion, deglaciation, etc., lead vertical movements (Jones 1980; Watts 2001). The classical isostatic concepts such as by airy and Pratt also considered vertical movements of blocks of crust by inter-block vertical dip-slip faulting (see Keary et al. 2009 for review). We therefore postulate that this set of faults results from post-eruption isostatic adjustments. Other authors concluded the same for onshore (Kailasam 1975, 1979; Watts and Cox 1989; Dessai and Bertrand 1995; Widdowson and Cox 1999; Campanile 2007; Campanile et al. 2008; Valdiya 2011) and offshore (Calvès et al. 2008) for the western continental margin of India.

Extension fractures

Extension fractures (Fig. 10), indicating tension normal to their strikes, are common in the alibag–Murud traverse. Their ~E–W trends (Fig. 10b) are fairly dominant near Murud (Fig. 2 for location). In field, extension fractures were identified on sub-horizontal outcrops by their sub-parallel strikes (following Hodgson 1961; Shah et al. 2007), nearly equal spacing (Eig and Bergh 2011; Gudmundsson 2011), and orthogonal abutting relation against another set of fractures/shear planes (Caputo 1995, 2010; Herman 2009; Park et al. 2010; Guidi et al. 2013). Though cooling fractures can be distinguished from polygonal fractures on sub-horizontal outcrops (a ydin and Degraff 1988; Schaefer and Kattenhorn 2004), the latter appear parallel and nearly equidistant on vertical sections (fig. 3 of lescinsky and Fink 2000) resembling extension fractures. Hence, we avoided vertical sections to identify them.

Other structures

a single, outcrop-scale pull-apart basin (Fig. 11) was found on a sub-horizontal outcrop at a rocky beach at nandgaon (refer Fig. 2 for location). The trend of the strike-slip segment, i.e., the "principal deformation zone" (PDZ; e.g., see

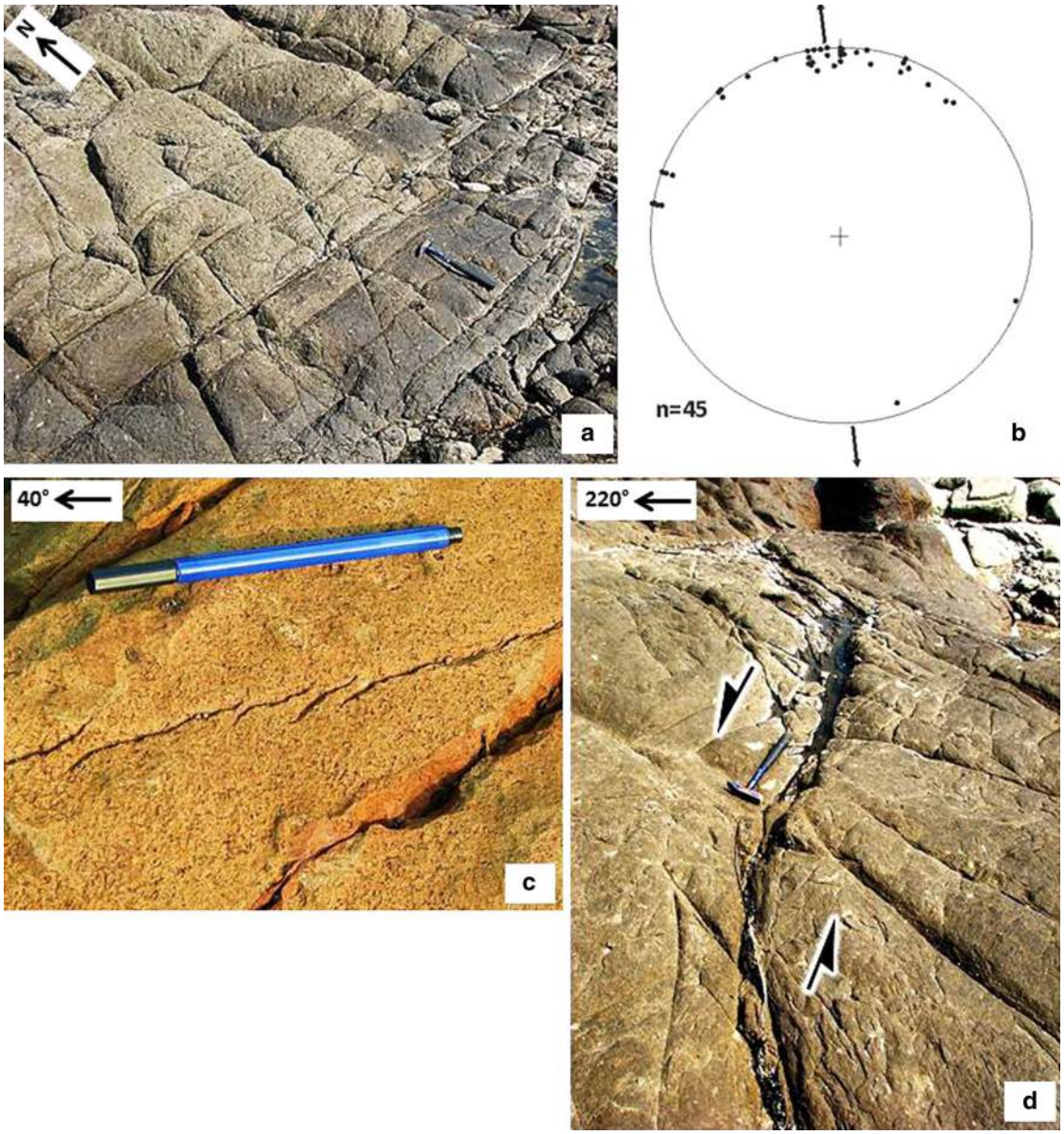

Fig. 10 **a** Extension fractures on sub-horizontal outcrops at Korlai–Kashid rocky beach (loc: 18°29′58.52″n, 72°54′13.89″E), refer Fig. 2 for locations. **b** Pole plots of extension fractures from the Kashid–Murud field area shows a n–S orientation of the minimum compressive stress (σ_3), marked by *black arrows*. lower hemisphere, equal area projection. **c** En-echelon fractures at aksa Beach (loc: 19°10′10.88″n, 72°47′21.44″E). **d** Horsetail structure at Murud (loc: 18°18′42.84″n, 72°57′32.80″E)

Dooley and McClay 1997) is 120°n with possibly normal faults striking ~160°n inside the basin. The normal faults would indicate a local ~nE–SW extension. But due to the absence of clear slip indicators, we did not use those for paleostress analyses. The pull-apart basin confirms strike-slip tectonics in the area. Rare en-echelon fractures (Fossen 2010; Davis et al. 2012) (Fig. 10c) and horsetail splays (Fossen 2010; Davis et al. 2012) (Fig. 10d) with ~EnE trend were noted near aksa and Murud (vide Fig. 2 for locations) and fits well with the other observations. Horsetail splays on sub-horizontal outcrops also indicate a strike-slip deformation (Davis et al. 2012). En-echelon fractures indicate extension perpendicular to them. When present along with other strike-slip indicators, they deduce shear sense (Fossen 2010; Davis et al. 2012).

Other than the pull-apart basin, normal faults were generally absent. notice that Dessai and Bertrand (1995) reported a single fault (40° dip toward E) without any shear indicator. Dessai and Bertrand's (1995) fault was not used for paleostress analyses in "Paleostress analyses" section.

Fig. 11 a mesoscale dextral pull-apart basin at nandgaon Beach (loc: 18°23′34.37″n, 72°55′14.47″E). The strike of the strike-slip fault is 120°n. The (possible) normal faults have strike ~160°n and have ~60° and ~50° toward E dips. Refer Fig. 2 for locations

no other authors reported normal faults from the western DlIP. Spheroidal weathering is dominant in Deccan trap rocks (Deshpande 1998; Bondre et al. 2006). Those, usually sub-circular and sub-elliptical curved fractures, were distinguished from sigmoidal *P*-planes, especially at aksa Beach. Fractures related to spheroidal weathering were ignored in tectonic interpretations. also, this study does not incorporate lava flow-induced local ductile shears (e.g., Misra 2014; Mukherjee 2013b) from Malshej ghat (location in Fig. 2) and along the Mumbai–Pune Expressway (unpublished observations by the first two author).

Remote sensing analyses

Remote sensing analysis and ground-truthing confirm deformation in regional scale. The sigmoid nature of the *P*-planes and their angular relation with the *Y*-planes, mentioned in "Brittle shears and striated fault planes" section, also decipher brittle shear senses on the satellite images.

Data and methods

We used false color composites of (1) landsat ETM+ Images-432 (RGB) (Fig. 12); and (2) Geoeye or Quickbird Images-123 (RGB). These were availed from Google Earth/World Wind (supplied by naSa at URl: http://worldwind.arc.nasa.gov/java/). World Wind specially has an "anaglyph stereo" mode to study the landforms, topography in stereographic vision (in three dimensions). This facilitates image interpretation. Both types of images were chosen to obtain clear and usable examples. Images with cloud and vegetation covers, etc., were discarded. The Deccan trap remains densely vegetated during and after the monsoon. Therefore, images during December to april were preferred.

a standard lineament analysis was performed manually (visually picked) on the ETM + images, without any minimum length function bias. a large number (> 2,000) of ~1–20 km long lineaments were mapped (Fig. 12). These lineaments were confirmed as geological features from Google Earth images by neglecting anthropological linear features such as roads and electric lines. The filtered out lineaments of geologic nature are grouped as follows.

1. Dykes: They most commonly appear elevated (correlated with topographical and digital elevation maps) and sometimes protrude into water bodies (Fig. 13a). These have been confirmed as dykes by ground-truthing (Fig. 13b) at few places and also from District

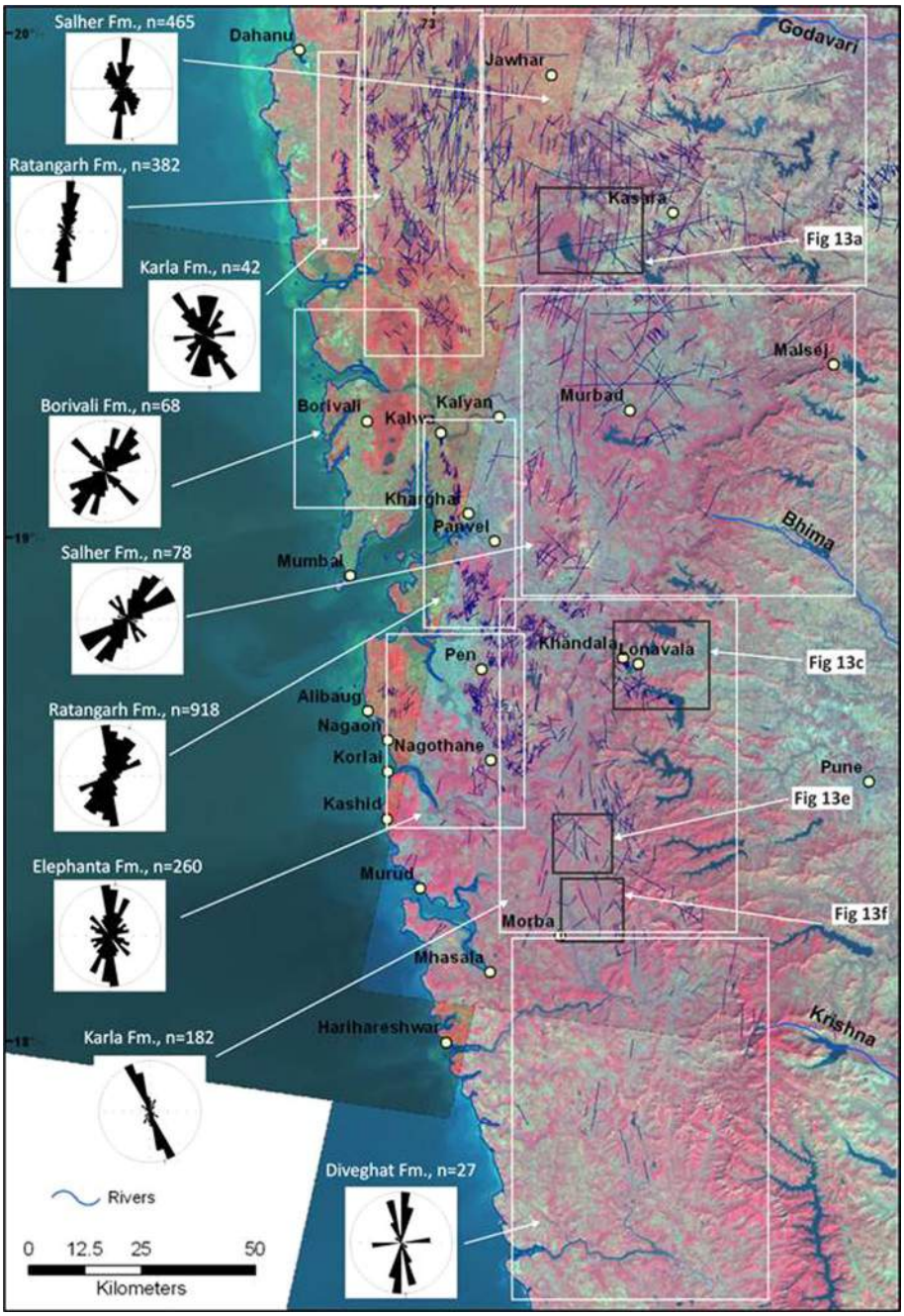

Fig. 12 Mosaic of landsat ETM+ images of the study area merged into 432 false color composite (FCC) image. *Bright red colors* dense vegetation; *greenish* to *greyish colors* barren areas; *blue*, *dark blue* to *black colors* water bodies. lineaments marked on this image (*blue lines*). *Rose* plots of the different areas (corresponding *white rectangles*) show the trends of the lineaments. *Small black rectangles* represent areas shown in Fig. 13 and numbered here in correspondence

Resource maps of Geological Survey of India (matching Fig. 2 with Fig. 12).

2. Unclassified: all of these cannot be identified confidently as dykes. But they can be subgrouped as follows.

   a. linear depressions, often water bodies form inlets through these lineaments (Fig. 13c).
   b. Densely vegetated linear features. These are much shorter than dykes. They are close-spaced, often in parallel clusters, and are almost equally spaced (Fig. 13e). Spacing varies from 500 m up to 2 km.
   c. These lineaments deflect rivers/channels locally into straight segments (Fig. 13f).

all these groups could not be confirmed from ground truth. This is because either they are inaccessible in field or sometimes those could not be located on ground due to surface weathering or soil cover. In one instance, ground truth proved a linear depression as a dyke (Fig. 13d). Dykes are normally more resistant than the country rock

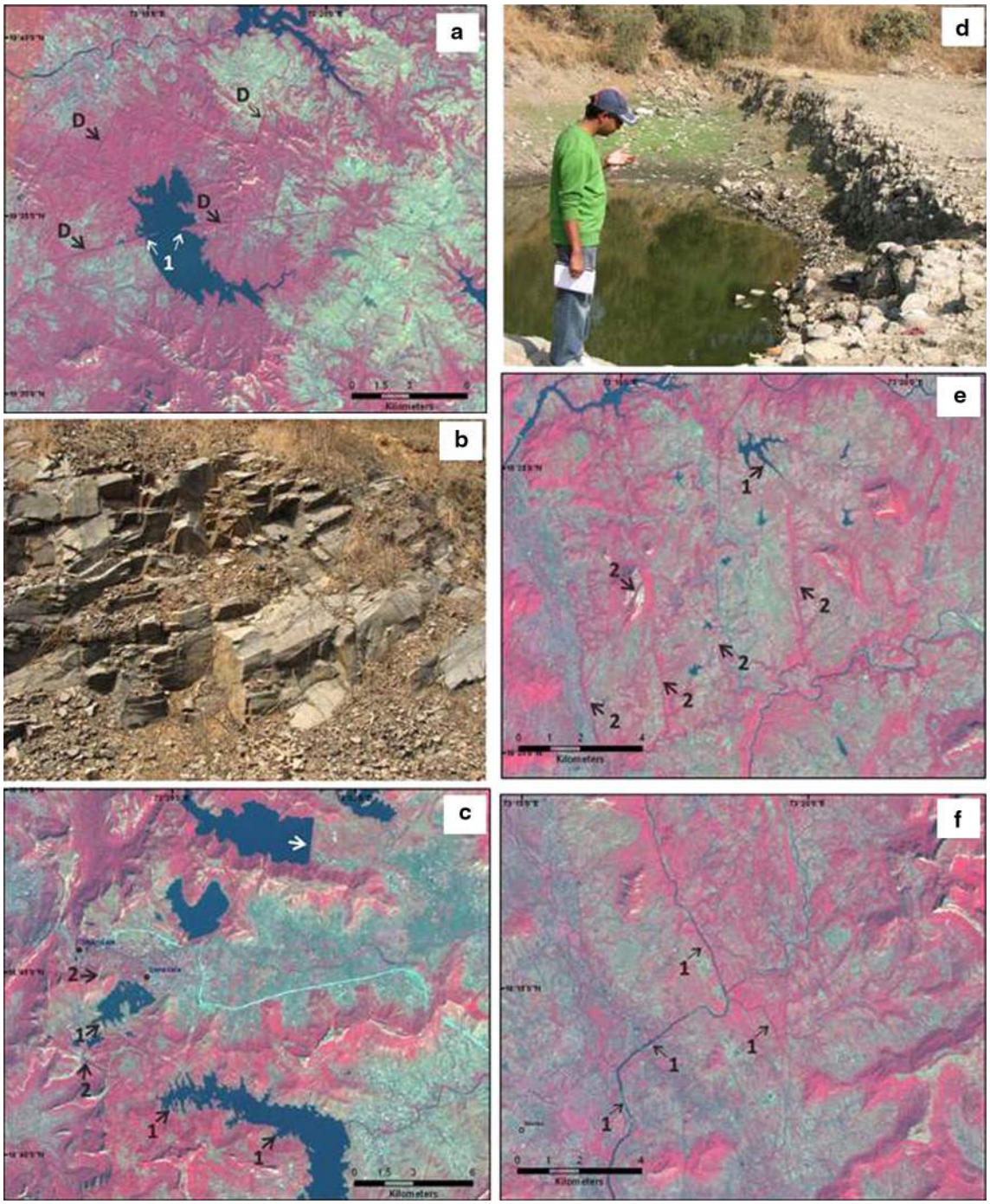

Fig. 13 lineaments mapped on the landsat ETM+ satellite data (Fig. 12) and field photographs. **a** D indicates dykes and (1) indicates the feature that the dykes form linear emergent ridges inside the water bodies. **b** One such dyke on sub-vertical outcrop. The dykes typically have three sets of rock cleavages more dominant near their boundaries. loc: 19°02′28.21″n, 73°03′05.21″E. **c** lineaments appear as depressions and associated with water bodies form linear inlets of water (1) and unassociated with water bodies (2). The *white arrow* shows a linear edge of a water body, which is a dam (checked on Google Maps!). The bright linear curved feature is the ~E–W trending Mumbai–Pune Expressway. **d** Field photograph of one such linear feature with depression. This is also a dyke, the boundaries of which bear three sets of rock cleavages. loc: 18°59′44.50″n, 73°02′36.48″E. **e** linear water bodies form inlets into lineaments (1) lineaments characterized by denser vegetation (2). **f** lineaments char - acterized by linear streams (1). See Fig. 12 for location of the satellite images

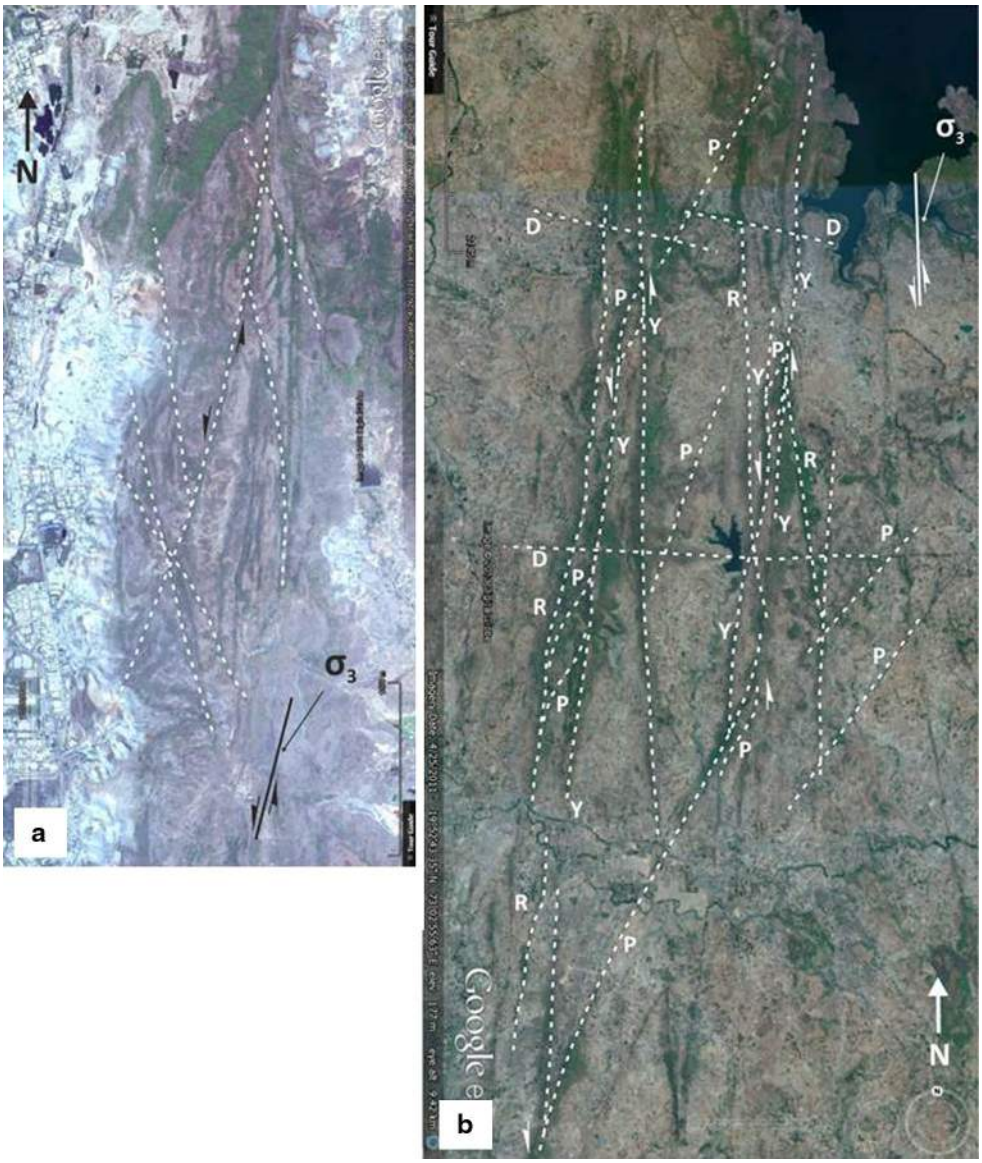

Fig. 14 High-resolution satellite image data taken from Google Earth. **a** The abutting relationship of the nW–SE lineament (dyke from ground-truth data) with the ~n–S lineament is clear and a possible slip is marked by *half-arrows*. **b** a conspicuous *P*- and *Y*-planes representation by lineaments. Both *P*- and *Y*-planes are most possibly dykes since these lineaments show linear positive elevation and are not depressions like other lineaments. The azimuth of the *Y*-plane matches with the *Y*-plane strike from outcrops. **c** an intricate network of lineaments represent *Y*–*P* (brittle shear), *R* (Riedel) planes indicate a shear zone. a few lineaments are marked by *dotted lines*. The possible sense of movement is represented by *white half-arrows*. 'D' indicates dykes possibly emplaced after shear since they crosscut all the other lineaments. The stream at south shows straight segments along the lineaments. **d** Part of the Jawhar–Malshej shear zone (this work, "Results" section) shows the lineaments (shear fractures or brittle shears) and the interpretation in **e**; settlements in *white circles*, *K* Khardi, *P* Patol, *S* Shirol; **e** *black half-arrows* mark the direction of movement, D are possibly dykes at a later intrusive phase because the cut across all other structures. The *Y*-planes trend ~120°n. For location of the image, see Fig. 2a–c and e has the possible range of the minimum horizontal stress orientation referred

and constitute elevated ridges. Intensely fractured and less resistant Deccan dykes were also reported (Peshwa and Kale 1988; Sabale and Meshram 2012). Thus, the unclassified lineaments, because of the above-mentioned characteristics, are likely to be dykes. However, the second group of lineaments can also be fractures, shear zones (see "Results" section), or brittle faults (compare Fig. 2 with Fig. 12). Previous authors used high-resolution images of Google Earth to distinguish lineaments from faults with displaced markers (e.g., fig. 6 in Viola et al. 2012). However, markers are too rare to recognize visible displacement on satellite images of the Deccan volcanics. The problem persisted

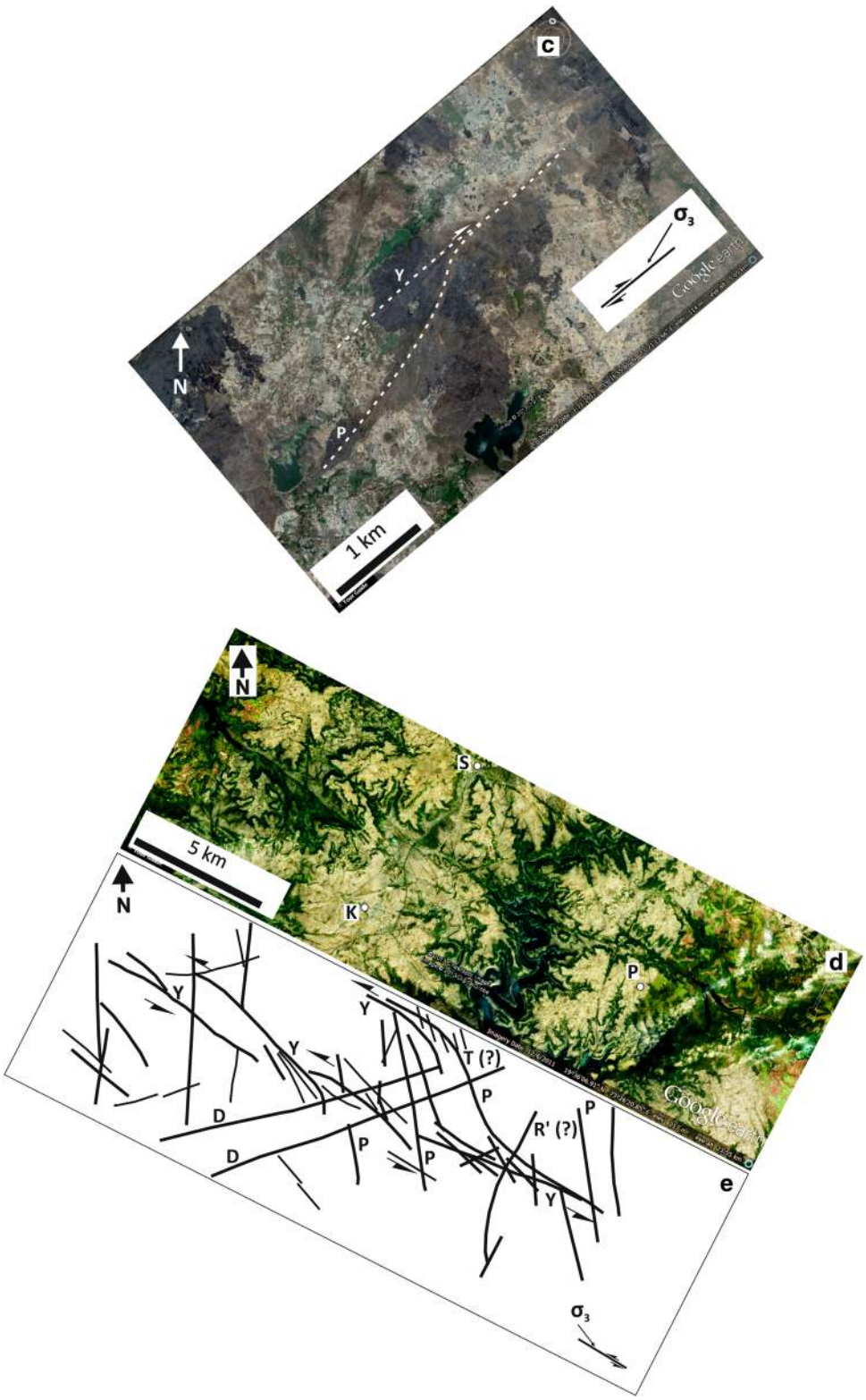

Fig. 14 continued

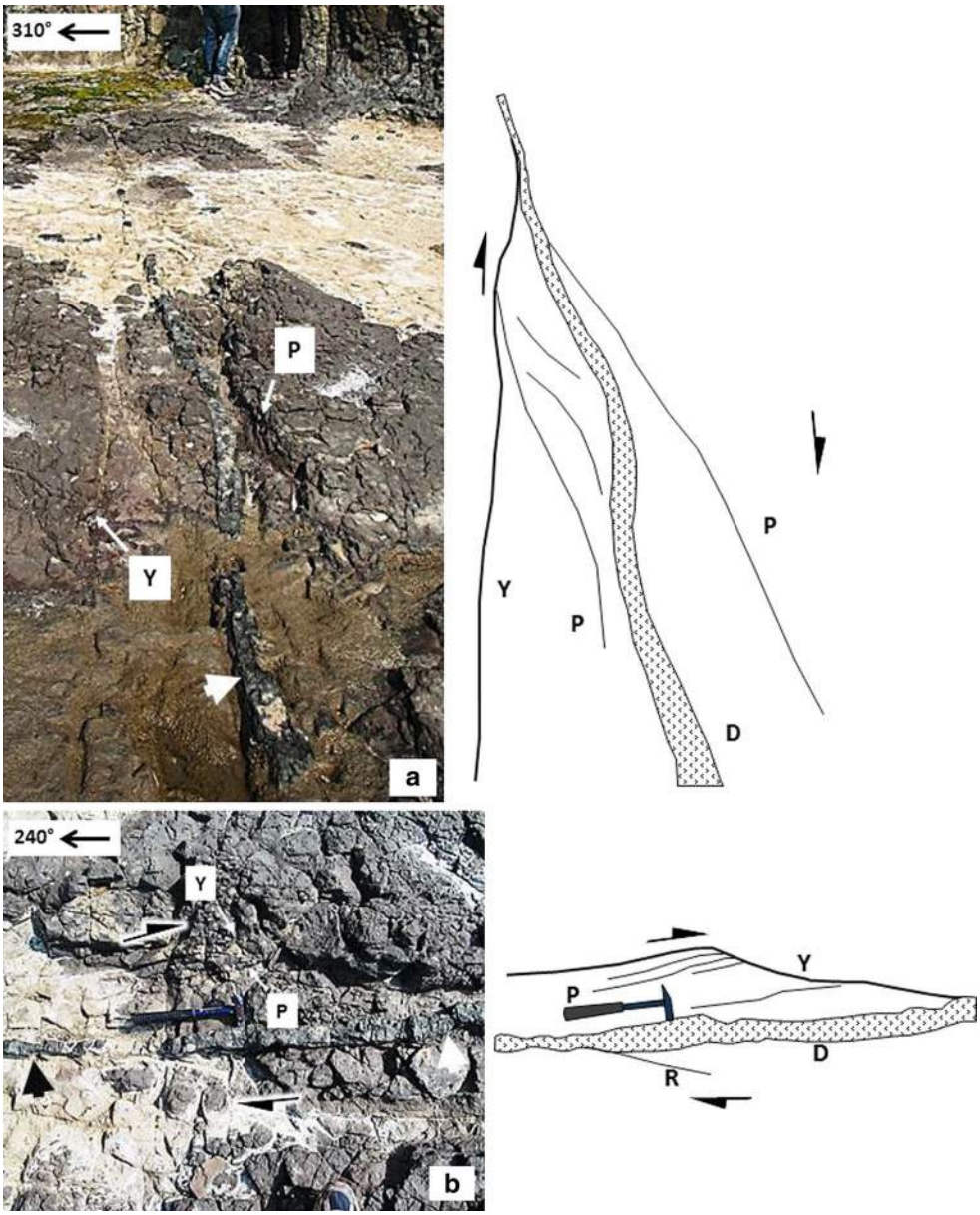

Fig. 15 Dykes at Murud show their association with the brittle shears on sub-horizontal outcrops **a** the dyke intruded between the *Y*-and *P*-planes and is parallel to the *Y*-plane, **b** *left* the dyke parallels the shear zone (the *Y*-plane); *line* drawing on *right* showing the relation of the dykes (D) with the main structures (*Y, P, R*). These form the Group II dykes of Hooper et al. (2010), which are coeval to or postdate. Refer Fig. 2 for locations

during field studies as well. Since the flows of Deccan traps are sub-horizontal (review by Valdiya 2010), slip of makers may remain undetected from satellite images. nevertheless, we recognized the displacement of one lineament across the other as a fault (Fig. 14a).

Previous authors did study Deccan trap lineaments (e.g., Peshwa et al. 1987; Dessai and Bertrand 1995; Bhattacharji et al. 1996; Widdowson 1997; Kundu and Matam 2000; Chandrasekhar et al. 2011) but on much lower resolutions. and, they could interpret only sparse lineaments of great lengths of tens of km. On the other hand, we infer ~50 m to 20 km long n–S lineaments, plausible dykes, from our study area.

This study analyses lineaments on higher resolution (30 m for ETM+ and 1 − 0.62 m for Google Earth) to interpret close-spaced and much smaller lineaments. additionally, this study attempts for the first time to identify brittle shears (*P*-, *Y*-, *R*-, *R*′-, *T*-planes) on high-resolution satellite images from the Deccan traps (Fig. 14b, c). Previous authors did not target these.

Geological Survey of India's maps, viz., the District Resource Maps (2001), delineated few large-scale faults. The Thane district map shows a series of nW-trending faults between the localities Jawhar and Malshej. These were confirmed as km-scale high-angle faults showing both dextral and sinistral shears with 10–30 m slip (Peshwa and Kale 1997). a close look at these faults on the Google Earth images revealed *P*-, *Y*-, and *R*-planes. The *Y*-planes trend ~nW–SE, which matches well with those documented from field ("Brittle shears and striated

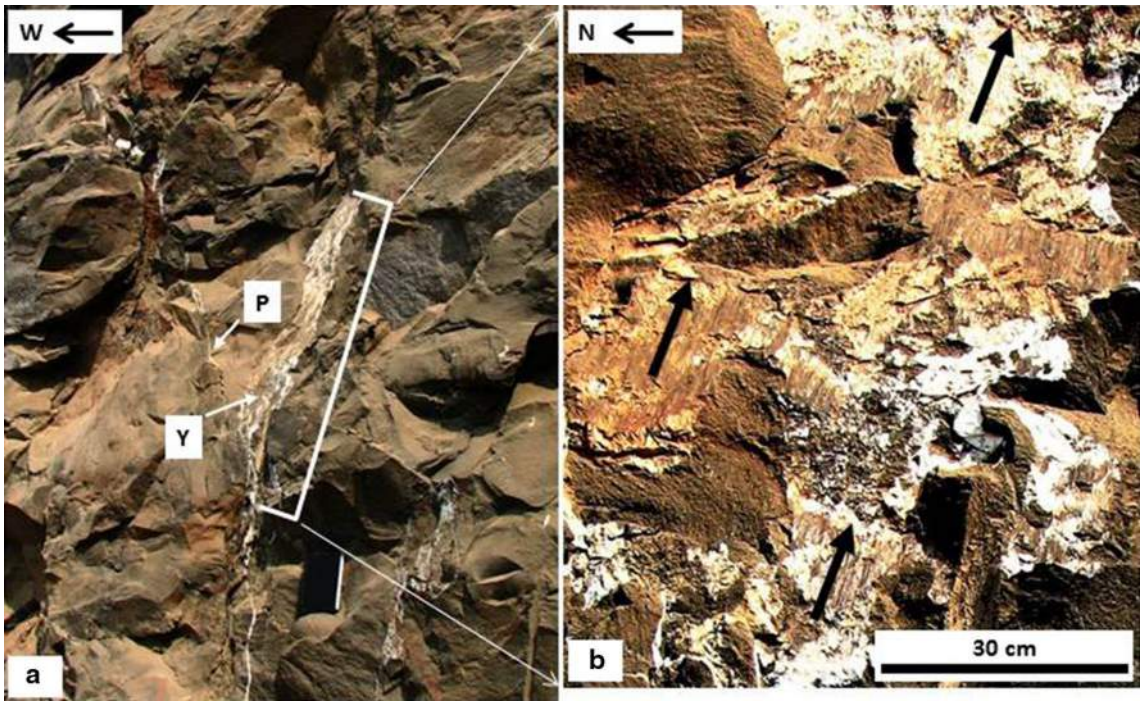

Fig. 16 **a** a sub-vertical brittle shear zone (sub-vertical outcrop) shows a mesoscale *P*- and a *Y*-plane at the Varcha–Owle quarries, near Panvel. loc: 18°59′23.22″n, 73°03′03.94″E. **b** The same *Y*-plane, polished and slickensided; the pitch of the slickensides is 90° on the *Y*-plane, showing the relationship of the brittle shears and the striated fault planes. *Black arrow* marks the sense of movement of the missing block. Refer Fig. 2 for locations

fault planes" section). This therefore appears to be a > 40 km long sinistral shear zone (Fig. 14d–e) through Salher Formation (the oldest Formation of the Deccan). We name this as the "Jawhar–Malshej shear zone." This ~nW–SE sinistral shear zone implied a ~n–S extension. Besides, most of the brittle shears we get from field trend ~nE–SW and are dextral. Those also imply a ~n–S extension.

Results

azimuths of lineaments mapped on the satellite images were divided into nine sets representing separate areas. These sets were then plotted into frequency–azimuth rose diagrams (Fig. 12). note that lineaments are not uniformly ~n–S trending.

almost all these lineaments we used represent dykes. notice the absence of the Jawhar–Malshej shear zone in the lineaments of Fig. 12. Smaller lineaments (e.g., the *P*-planes) cannot be picked up at this resolution. These dykes do not follow the general ~n–S trend throughout the coastal DlIP around Mumbai as found by previous authors (Beane et al. 1986; Sheth 2000; Vanderkluysen et al. 2011 etc.). additionally, there are many ~E–W lineaments (Fig. 12), which are dykes (compare Fig. 2).

The dykes in the study area (Fig. 2) trend ~n–S north of Kalyan and change abruptly to a dominantly nE–SW trend at south. Swing of dykes was not described previously. Comparably, lineament mapped in this study (Fig. 12) is dominantly ~n–S north of 19°n latitude within the older Kalsubai Subgroup. South of 19°n, these lineaments reduce at the cost of nE–SW and some nW–SE lineaments. n–S lineaments vanish in Salher, Borivali, and Karla Formations (rose plots in Fig. 12). a few E-trending lineaments are also present throughout the area (e.g., D in Fig. 14c, e). Those appear to be last-stage (post-64 Ma?) dyke intrusion because they seem to cut across all other dykes. There are almost no dykes/lineaments S to ~18°n (Figs. 2 , 12). Interestingly, the trend of lineaments (mostly dykes) match with those of the shear zones/striated faults (compare dykes and faults in Fig. 2; detailed in "Regional geology" section).

Remote sensing revealed slip (Fig. 14a), *P*–*Y* planes (Fig. 14b–e), Riedel shears (*R* and *R*′) (Fig. 14c), and brittle shear zones (Fig. 14d). note that *P*–*Y* planes (for brittle shears) cannot distinguish from *C*–*S* planes (as in ductile shears) on satellite images since both the *S*- (and the *P*-) planes sigmoidally merge with the *C*- (and the *Y*-) planes. Since only brittle shears persist in the field (see "Structural geology" section) from same areas as shown in satellite images, we confirm those on the images to be *P*–*Y* planes.

Table 2 Orientations of stress tensors derived by visualization of the Gauss function (VGF) method and azimuth of the maximum horizontal extension (SH_{min}); azi: azimuth, Pl: plunge, Φ, R: shape parameter of the stress ellipsoid (see "Results of inversion" section for details), n = number of faults/brittle shears considered; Q: quality of the tensor (see "Results of inversion" section). See Fig. 17 for a map with maximum horizontal extensions

Formation	location	SH_{min}	σ_1		σ_2		σ_3		Ratio	Φ	R	n	Q
			azi.	Pl.	azi.	Pl.	azi.	Pl.					
Borivali	aksa	346	072	02	255	88	160	00	1.01:0.17:0.07	0.1	0.1	62	1
	Kanheri	355	075	00	169	86	345	04	0.89:0.48:0.06	0.5	1.0	10	1
Diveghat	Harihareshwar	338	244	02	136	85	335	05	1.04:0.17:0.07	0.1	0.1	26	1
	Elephanta	338	074	00	169	86	343	04	0.99:0.35:0.07	0.3	0.4	9	1
	Korlai–Kashid	346	081	00	173	87	351	03	0.99:0.25:0.07	0.2	0.3	27	1
Elephanta	nandgaon	359	085	00	177	85	355	05	0.92:0.41:0.07	0.4	0.7	25	1
	Janjira	183	280	01	175	86	011	04	0.94:0.33:0.07	0.3	0.4	35	1
	Murud	346	092	00	186	85	003	05	1.01:0.17:0.07	0.1	0.1	28	1
	Mhasala	183	084	00	175	86	354	04	0.94:0.33:0.07	0.3	0.4	41	1
	nagothane	357	273	06	100	84	005	01	0.71:0.71:0.05	1	CO	25	1
Karla	Morbe	207	103	00	193	84	014	06	0.94:0.5:0.07	0.5	1.0	12	1
	Turbhe	253	354	06	180	84	83	01	0.87:0.55:0.06	0.6	1.5	5	3
	Kharghar Hills	285	001	05	125	81	270	08	0.9:0.48:0.06	0.5	1.0	24	2
	Varcha–Owle	290	013	03	126	83	282	06	0.88:0.55:0.06	0.6	1.5	18	3
U. Ratangarh	nhava Phata	322	053	01	237	89	140	00	1.1:0.18:0.08	0.1	0.1	47	1
	Chirner1	337	056	29	192	62	314	22	1.11:0.08:0.08	0	0	25	1
	Chirner2	332	255	40	024	37	139	30	1.06:0.27:0.08	0.2	0.3	12	1
	Kharpada	358	248	04	118	83	339	05	0.81:0.59:0.06	0.7	2.3	10	1
	Murbad	297	007	26	216	61	102	12	0.97:0.43:0.07	0.4	0.7	3	3
l. Ratangarh	Bhatan	288	037	02	143	81	305	08	0.76:0.69:0.05	0.9	9.0	6	2

Interpretations and implications

Based on the above observations coupled with field evidences in "Dykes" section, we interpret that the dykes of ~n–S trend in the n and ~nE–SW and ~nW–SE in the S emplaced along shear fractures. These fractures existed when magma intruded. Such an interpretation was also proposed by Peshwa and Kale (1997), who suggested that flexuring of the crust during rifting and loading of sediments in the offshore areas opened n–S trending fractures, where the dykes intruded later. The best and direct evidence of this is found in Fig. 14b. Here, one lineament meets tangentially the other. The former is a dyke. The latter ~40°n lineament is also elevated, elongated, and linear. This geometry is best explained as dykes intruding preexisting *P*–*Y* planes. In field, the dykes strongly follow the shear zones (Fig. 15a, b; see also Hooper et al. 2010). They also either occur between a *Y*-plane and a *P*-plane of a single brittle shear zone (Fig. 15a, b) or intrude preexisting fault planes (also see fig. 5 of Dessai and Bertrand 1995).

Emplacement of dykes along preexisting shear zones contradicts their general emplacement modes. Dykes emplace perpendicular to the direction of minimum compressive stress (σ_3) and parallel to the maximum compressive stress (σ_1) (Gudmundsson 1984, 2011). This resembles mode-I fracturing (Fossen 2010). Dykes emplace where the tensile strength of the rock is least (Gudmundsson 1984). Preexisting shears/tensile fractures are planes along which the tensile strength almost vanishes. Thus, dykes usually follow existing fractures in country rocks. However, dyke intrusions always have dilation components since they forcefully push the country rock almost perpendicular to themselves. Mentioned in "Dykes" section, the dykes in the study area can be classified into three groups. One group of dykes predates the deformation and the other two are either coeval or are post-deformational (also Hooper et al. 2010). Dykes, thus, need to be studied carefully before assigning tectonic extension in response to their emplacements. Dykes identified in satellite images crosscut each other at numerous places. However, these images could not deduce the relative timing of intrusion. Geometry and emplacement of tabular magmatic bodies are controlled by complicated internal (magmatic) and external (tectonic) stresses (Hutton 1992; Glazner et al. 1999; Correa-Gomes et al. 2001). Watkeys's (2002) figure 11 represents the intrusion of dykes along preexisting *Y*-, *P*-, *R*-, *R*′-, and *T*-planes with a dominant emplacement through *Y*-planes at Karoo volcanics, South africa. That dykes intrude preexisting or active shear zones were also observed elsewhere, e.g., Washington (Cater 1982); the Middle Jurassic Concón Mafic Dyke swarm at Chile (Creixell et al. 2006); Paleogene dykes on livingstone Island, antarctica (Kraus et al. 2010); Sierra de San Miguelito, central Mexico (Xu et al. 2012).

The Jawhar–Malshej shear zone is confirmed to be a fault from Peshwa and Kale's (1997) work. They found dextral and sinistral displacement (~10–25 m) of n–S-trending dykes along the fault zone and also vertical slip of basalt flows near the Khardi settlement (location in Fig. 14d). The ~nW–SE trend of Jawhar–Malshej shear zone appears to be a northernmost continuation of the nW–SE Kurduwadi lineament, which is in turn a manifestation of the Precambrian Wadi shear zone (Peshwa and Kale 1997). So, the dextral Wadi shear zone was active before the DlIP emplacement, reactivated as the sinistral Jawhar–Malshej shear zone during India–Seychelles rifting and activated again possibly since Pliocene (Dole et al. 2000; Babar et al. 2012).

lineaments that were identified with confidence are either shear fractures (e.g., Fig. 14c, d) or dykes intruded into shear fractures (Fig. 14b). Both of them yielded paleostress orientations (Fig. 14). This is a key to understand the regional paleostress field. The minimum horizontal stress axis (σ_3) was marked on the satellite images (Fig. 14). appendix 1 describes the procedure. The exercise reveals ~nW to ~nE trending σ_3. These trends are ubiquitous where a large number of interpretable lineaments exist, e.g., Fig. 14d–e. The deduced orientations also match with those derived from the field-based paleostress study ("Paleostress analyses" section). Remote sensing analyses from the northern areas (viz., Dahanu and Jawhar: see Fig. 2 for locations) were also obtained (Figs. 2, 14d–e). Remote sensing study was used to confirm the regional nature of the deformation. This was done by matching the trends of the shear zone with those obtained from the field. approximate stress orientations were interpreted from the lineaments mapped (Fig. 14).

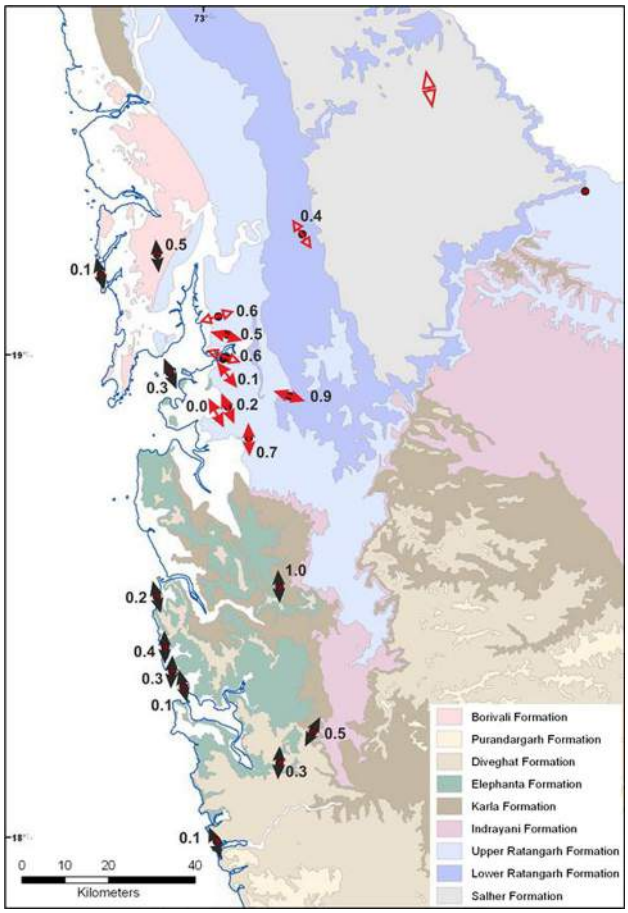

Fig. 17 Positions of the maximum horizontal extensions (SH_{min}) on map overlapped on the Formations map. For details on the tensors and SH_{min} azimuths, see Table 2 and Fig. 18. The *blank arrows* indicate a quality factor of 3. The large arrow near nE indicates the extension direction obtained from remote sensing analysis for the Jawhar–Malshej shear zone (see "Remote sensing analyses" section and Fig. 14e). Compare with Fig. 2 for locations. *Red arrows* azimuths for older Formations (of the Kalsubai Subgroup); *black arrows* azimuths for younger Formations. The *numbers* alongside the arrows are *location specific* Φ values for the stress tensor

Paleostress analyses

Data and methods

We examined > 60 outcrops where ~30 outcrops at 19 locations provided quality data used here. Paleostress analyses and related inversion require the following data sets: (1) "azimuth" and "dip" (or attitude) of the fault planes, i.e., *Y*-plane for brittle shears and *M*-plane for Riedel shears; (2) "lineation" (or the attitude of the slip vector, e.g., pitch of the striae of slickensides on faults; (3) "type:" slip sense normal, reverse, dextral sinistral; and (4) "reliability:" confidence of the measured data, viz., uncertain, possible, probable, and confident (e.g., Žalohar and Vrabec 2007; Sippel 2009; Žalohar 2009; Sippel et al. 2010; Zachariáš and Hübst 2012). Terminologies mentioned inside "double inverted commas" are as per Žalohar (2009). For slickenside-bearing fault planes, attitude of fault planes and pitch of lineations on fault planes were measured following conventional shear sense indication techniques of Hancock (1985), Petit (1987), and Doblas (1998). Those are the "positive" and "negative" smoothness criteria, orientation of elongated grooves of the fault planes, angular relationships between fractures and fault planes, etc. as mentioned in "Brittle shears and striated fault planes," steps and asymmetric elevations are a kind of slickensides (Doblas 1998). a line perpendicular to the crest/hinge line of asymmetric elevations was taken as the slip vector. This line therefore resembles striations/slickensides for steps and asymmetric elevations (Fig. 8c). The vector has a direction along which a gently moving hand feels smooth on the fault plane.

The slip vector is usually perpendicular to the line of intersection between the *Y*- and the *P*-planes and lies on

the *Y*-plane (Supplementary Fig. S1). This relation was tested on a number of (semi-) ductile shear zones (*C*- and *S*-planes) and was found to closely match the actual striae present on the surface (Srivastava et al. 1995). Other workers (Marquer et al. 1996; Ciancaleoni and Marquer 2006; Menegon and Pennacchioni 2010) also confirmed this. We noticed field evidences for this relation at the Varcha–Owle quarries (Fig. 16a, b) where slickensides have ~90° pitch on the *Y*-plane, that is, the intersection between the *Y*- and the *P*-planes parallels the strike of the *Y*-plane. We measured the attitude of both *Y*- and *P*-planes and derived the attitude of their line of intersection (l1). Then, we obtained the attitude of the line l2 that lies on the *Y*-plane and is perpendicular to l1 (Supplementary Fig. S1). We infer slip sense from the l2 lines and the curved *P*-planes. The actual slip may differ from that calculated by the above method (Srivastava et al. 1995), but not significantly. For example, a brittle shear with vertical line of intersection (l1) between *P*- and *Y*-planes can never be dip-slip. Similarly, asymmetric elevations with vertical crests would not represent a dip-slip fault. also, for vertical faults, the calculated "maximum horizontal extension"/"minimum horizontal compression" (SH_{min}) shows small deviation. We trialed a dextral vertical fault plane with 45° strike and varying pitch, keeping all other parameters (azimuth: 135°, dip: 88°, shear sense: dextral, reliability: confident) constant. The resolved SH_{min} for the said fault plane for pitch 2°, 5°, 10°, 15°, and 20° are 322°, 329°, 335°, 330°, and 330°, respectively. It shows that for sub-vertical fault planes, as a special case, we can use this slip vector calculation effectively. Moreover, using a large population of faults/brittle shears at one location, such as our case (Table 2), the errors can be minimized statistically.

For the strike-slip faults, the *P*-planes are sub-vertical (Fig. 3) and at low angles (10–30°) to the *Y*-planes (also sub-vertical). For the dip-slip brittle shears, their dips range 50–80°. Thus, the lines of intersection between the *P*- and the *Y*-planes either dip steeply or are sub-vertical (~75–90°) in the former case. In the second case, the lines are sub-horizontal (~0–15°).

Results of inversion

Slip vectors or "lineation(s)" directly measured from slickenside lineations or calculated from intersection lines, as mentioned in "Data and methods" section, are used to resolve the paleostress tensors following the "Wallace–Bott hypothesis" (Wallace 1951; Bott 1959). The hypothesis states that the maximum resolved shear stress (τ_{max}) along a fault plane parallels the observed slip directions/slip vectors. The main assumptions are (1) the remote stress tensor is identical spatially and also homogenous; (2) the slip on the fault plane should represent the maximum resolved shear stress (τ_{max}); (3) slip has to occur on faults of varied attitudes in the area but ought not to interfere. Put another way, the respective slips of all the faults are to be mutually independent (nemčok and lisle 1995; Twiss and Unruh 1998; Kaven et al. 2011; lacombe 2012). The first two

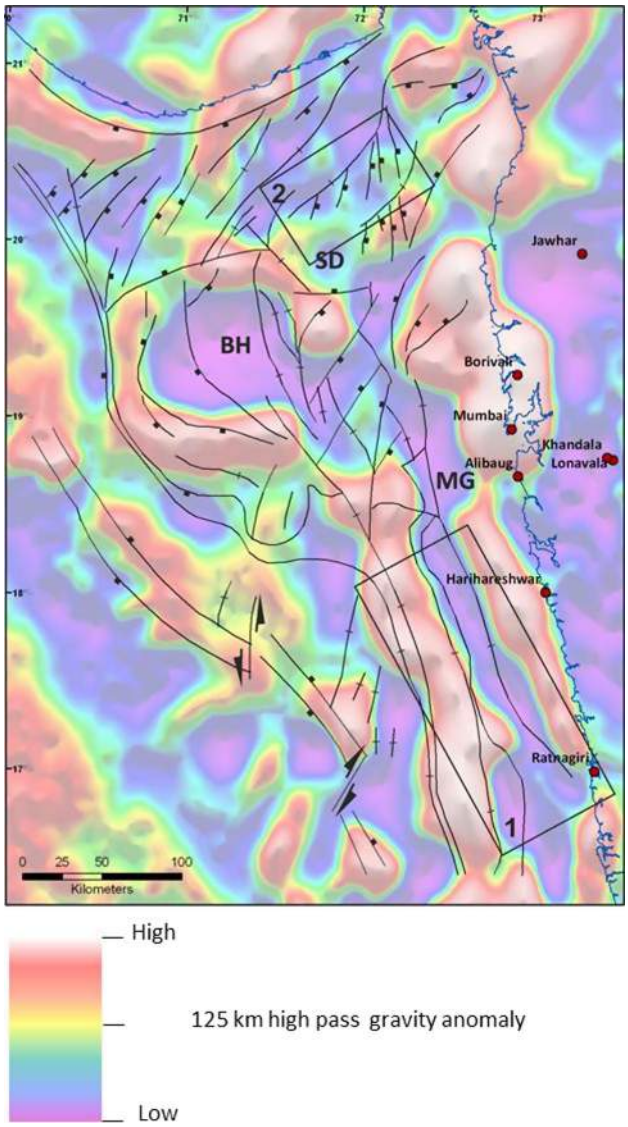

Fig. 18 Fault map at Deccan trap level (after Verma et al. 2001; naik et al. 2006) around Bombay (Mumbai) High (BH) area shows strike-slip architecture overlapped on 125 km high-pass gravity anomaly data: *Blue*/*purple* for lowest and *white*/*pink* for highest gravity anomaly values (Satellite Free air gravity anomaly data from Sandwell and Smith 2009). The dips of the faults were reinterpreted from geological cross-sections from Basu et al. (1980), Roychoudhury and Deshpande (1982), Gopala Rao (1990), Verma et al. (2001), and naik et al. (2006). Surat depression (SD) forms possibly a part of the transtensional segment. The elongated Mahim Graben (MG) that continues till Ratnagiri offshore area possibly forms the *Principal Deformation Zone* (*the area numbered 1*). n of Surat depression, the *area numbered 2* also indicates a possible horsetail structure

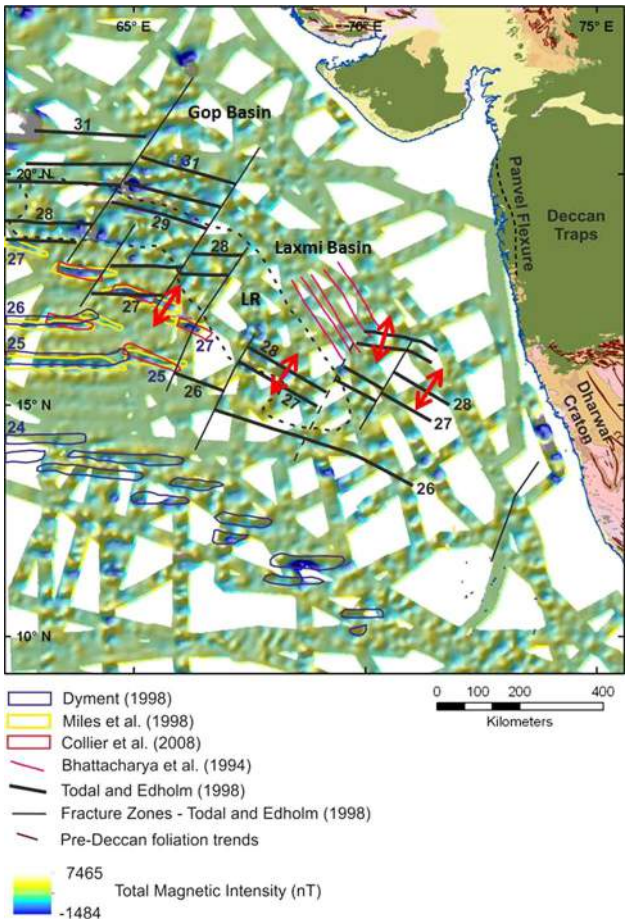

Fig. 19 Total magnetic intensity map with magnetic seafloor spreading anomalies interpreted by previous authors (mentioned at *legend*). The *numbers* in *bold* black are magnetic chrons interpreted by Todal and Edholm (1998) and those in *bold purple* by other authors (27 = C27n, 26 = C26n, etc.). *Red arrows* plate movement directions. Collier et al. (2008) presented data of previous authors in their map. This diagram is plot of Collier et al's (2008) data on that map. See "Discussions and conclusions" section for details

assumptions hold for natural cases within a limited time. For the third, cluster analyses sort out "phases"/"clusters" in a heterogeneous/polyphase fault-slip data (e.g., nemčok and lisle 1995).

at least four such data sets of variable orientation in a particular location estimate a "reduced stress tensor" (Carey and Brunier 1974; angelier 1979, 1984, 1994). These are (1–3) the orientation of the three mutually orthogonal stress axes σ_1, σ_2, σ_3 ($\sigma_1 \geq \sigma_2 \geq \sigma_3$) (4) the stress ratio: $\Phi = (\sigma_2 - \sigma_3)/(\sigma_1 - \sigma_3)$, where $0 < \Phi < 1$ (angelier 1989; angelier et al. 1990). The stress ellipsoid is oblate for $\Phi > 0.5$ and prolate for < 0.5. a different parameter "R" ($= \Phi/1 - \Phi$) is also used (armijo and Cisternas 1978; angelier 1989; lisle 1989) that ranges 0 to ∞. Célérier et al. (2012) and lacombe (2012) recently reviewed paleostress estimates from fault-slip data.

We used the computer program T-TECTO (version 3.0; author: J. Žalohar) that uses the Gaussian algorithm (Žalohar and Vrabec 2007) to calculate the orientations of the stress axes. The T-TECTO program was employed because it provides visualization of strains and stresses by both geometric and statistical inversion techniques. Its clustering program sorts out deformation phases (e.g., Smith et al. 2012). The program also flexibly incorporates fault planes with dubious striae and tension fractures (e.g., luther et al. 2009). The program uses right dihedra method (RDM of angelier and Mechler 1977; angelier 1989) to calculate the strain tensor. It then applies the Gaussian function to invert and resolve the reduced stress tensor. We used these methods to invert our field data. We used the Gaussian parameters of $s = 30°$, $\Delta = 60°$, $q_1 = 60°$, and $q_2 = 20°$ (vide appendix 2 for detail), depending on the rock type (usually basalt) and standards mentioned in Žalohar and Vrabec (2007) and Žalohar (2009). The Q factor in Table 2 represents quality for the paleostress inversion, viz., 1 = Very Good, 2 = Good, and 3 = Fair. The quality criterion depends on the field evidences, e.g., number of striated faults and confidence in the shear sense of the fault planes. Table 2 lists stress inversion results of the 19 locations (locations in Fig. 2). Supplementary Table 1 presents geographic coordinates of data collected.

The data were sorted according to location to corroborate with the ages of the Formations (stratigraphy in Table 1 and Fig. 2). We then performed unsupervized cluster analyses (like Etchecopar et al. 1981; nemčok and lisle 1995; Yamaji 2000; Yamaji et al. 2006; Žalohar and Vrabec 2007; reviews by Célérier et al. 2012) to automatically separate fault clusters using the Gaussian function in T-TECTO (Žalohar and Vrabec 2007). We accepted inversions only when the misfit angle "α" (see appendix 2 for details) was < 30° (nemčok and lisle 1995). Most of the misfits ranged 10–15°.

Vertical dip-slip faults and ~n–S brittle shear zones plotted as different clusters (see the plotted "problematic faults:" PF in Supplementary Fig. S2). We thus considered them as deformations different from the rest of the faults/shear zones. The ~n–S trends of these vertical, dip-slip faults match with those in figs. 3 and 6 of Dessai and Bertrand (1995). Paleostress tensor calculations on this fault cluster yielded a σ_3 roughly perpendicular to the fault plane. This is an unrealistic solution because there can be almost no extension on these sub-vertical faults. Though we resolved stress tensors for these faults as well, we avoided them in tectonic interpretation. Faults belonging to a single cluster come from aksa, Turbhe, Kharpada, nandgaon, Elephanta, Janjira, nagothane, Morbe, and Bhatan (Fig. 2 for locations). Two clusters of faults are deciphered at Kanheri, Kharghar, Varcha, nhava, Korlai–Kashid, Murud, Mhasala, Harihareshwar, and Murbad (locations in

Fig. 2). Only at a single location Chirner, shown in Fig. 2, three clusters of faults were interpreted (Supplementary Fig. S2). no correlation exists between the ages of these Formations and the number of clusters. The separated out cluster of problematic faults also consist of sub-horizontal striae. These are faults that misfit the solution (Supplementary Fig. S2).

We calculated *P*–*T* axes (*P* = compressive; *T* = Tensile) for each fault and stress axes through geometrical RDM and statistical visualization of the Gauss function (VGF) method (Supplementary Fig. S2). Thus, we compared the geometrical and statistical inversions for same fault populations. These solutions are mutually comparable, with occasional mismatch at the locations Turbhe, Varcha–Owle, Chirner, Morbe, Bhatan, and Murbad (Supplementary Fig. S2; see Fig. 2 for locations). This misfit is due either to data scarcity or large spread in the data points on the stereo plot. a large spread is possible because of variable pitches of slip vectors on the fault planes. The σ_2 axes are sub-vertical, indicating a strike-slip deformation. The *P*–*T* axes provided the contribution to the strain for each of the faults. Further, we computed the SH_{min} for all the locations (Fig. 17). Since these are strike-slip faults, the SH_{min} orientations gave the extension direction, and we use those for the geodynamic interpretation.

The paleostress tensors (Table 2 and Supplementary Fig. S2) thus obtained for shear zones show a wide variation in SH_{min} and in the trend of σ_3. The σ_3 varies mainly from ~nnW–SSE (at Chirner, Harihareshwar, nhava Phata, Murbad, Bhatan, and Kharghar) to nE–SW (at Morbe), and one ~E–W trend (at Turbhe) (Fig. 17). a few ~n–S trends were found especially at Kanheri, nandgaon, Janjira, Mhasala, and nagothane. We grouped the stress tensors as follows. a group belongs to the older Formations (Ratangarh Subgroup) and another to the younger stratigraphic units (Karla, Elephanta, Diveghat, and Borivali Subgroups) (Fig. 17). These two groups are not homogeneous in terms of SH_{min} orientations within and resemble in tensors across the clusters (see Table 2; Fig. 17). Rather, the tensors trend nnE to nnW along the coast and show nW or nE orientations away from the shore. The ~E–W set at Bhatan, Varcha–Owle, and Turbhe might be by insufficiency/large spread of the data points. That the shear is indeed a strike-slip one was inferred confidently from visual analysis of deformation structures in the field. The most important outcome of this exercise is that the trend of the extension direction, i.e., the σ_3 axis, is ~n–S or ~nnW–SSE in general, and not E–W. Thirteen out of 20 tensors trend ~150°n. The orientations are consistent for a ~n–S extent for > 150 km and ~70 km along E–W as traced in the field ("Structural geology" section) and beyond by remote sensing ("Remote sensing analyses" section).

Discussions and conclusions

as mentioned in "Introduction" and "Tectonics" sections, the ages of the Deccan basalts prove that most (> 80 %: Chenet et al. 2007) of the volume of the magmatic products emplaced in the initial stages of volcanism (i.e., by ~65.5 Ma) before the India–Seychelles rifting (~63.4 Ma: Collier et al. 2008). also, the dyke relations prove that the breakup started only after bulk volcanism (Hooper et al. 2010). and the deformation in the rocks should represent the India–Seychelles rifting. The far-field stresses, responsible for the rifting, activated presumably much before the DlIP erupted (Courtillot et al. 1999), possibly as early as ~80 Ma (Todal and Edholm 1998). However, sufficient thinning was not achieved when the bulk volcanics emplaced (Saunders et al. 2007).

The study area was dextrally strike-slip faulted along sub-vertical planes, and we designate this as the "Western Deccan strike-slip zone." Some isostatic-related vertical dip-slip faults are also present. low dipping (< 60°) normal faults occur at orthogonally rifted margins with the strike of the normal faults perpendicular to the direction of maximum extension (σ_3) (e.g., Destro et al. 2003). Such normal faults do not usually occur here. an outcrop-scale pull-apart basin was also found in the field (Fig. 11). Repeatedly found were *Y*–*P* planes of brittle shears, asymmetric elevations with vertical crests, vertical fault planes with sub-horizontal slickensides, etc. Riedel shears (*R* and *R*′) connote strike-slip faulting. Sinistral reverse shear sense was found locally. Such limited reversals were noted from many shear zones in the world (e.g., Simpson and Schmid 1983; Malavieille 1987; Davis and lister 1988; Spencer 1984; Reynolds and lister 1990; Koyi et al. 2013 for review). Concise studies on reversal are lacking, and we cannot comment the tectonics of sinistral shear. The WDSZ persists for > 150 km along n–S (from aksa to Harihareshwar) and ~70 km along E–W (locations in Fig. 2).

For andersonian normal faults and strike-slip faults, σ_3 equals SH_{min}. For andersonian thrust faults, σ_2 is the SH_{min}. The SH_{min} is the horizontal component of σ_3. The resolved minimum compressive stress (σ_3) for these faults/brittle shears trends widely from ~nW–SE to ~nE–SW (Table 2; Figs. 18, 19). The older Formations of Kalsubai Subgroup show SH_{min} orientations of ~nW–SE to ~n–S (Fig. 17) along with nW to nE faults/brittle shears (Supplementary Fig. S2). However, faults/brittle shears reorient S to younger lonavala and Wai Subgroups into a dominant ~nE–SW and minor ~nW–SE with ~nnW–SSE σ_3. We also had one ~nE-oriented σ_3 at Morbe (Fig. 17). This orientation of the faults/brittle shears is also found in the youngest Formations in the n part of the study area (Salsette Subgroup rhyolites at aksa Beach). Here, σ_3 resolves ~n–S (Fig. 17). The dykes and lineaments show the same

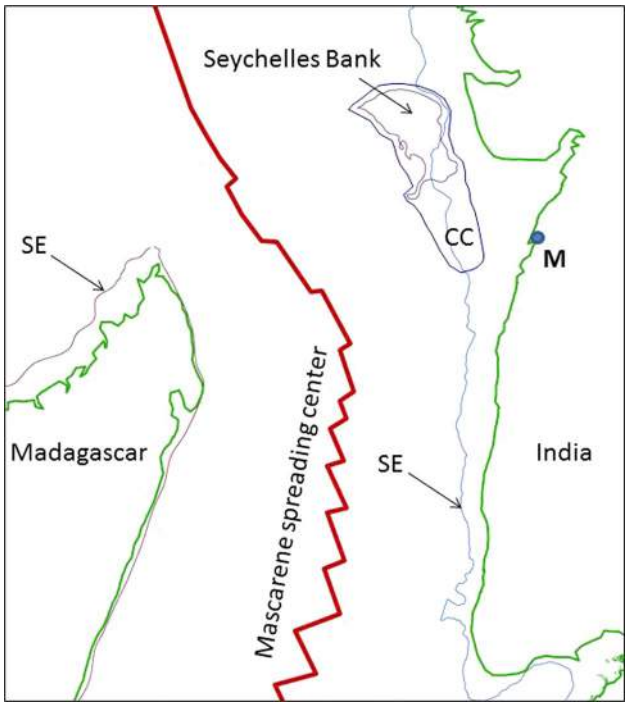

Fig. 20 Plate tectonic reconstruction map, a schematic diagram, shows the position of India–Seychelles bank and Madagascar at 65–70 Ma (after Seton et al. 2012). CC: extent of continental crust around Seychelles (after Plummer et al. 1998); SE: present-day indicative shelf edge; *M* Mumbai

swing in trend from a dominant ~n–S in the n to a ~nE–SW (some n–S) in the S (Figs. 2, 12). Thus, two possibilities arise viz. (1) indeed the stress reoriented with time and (2) the stress orientation varied in space. Since we did not observe the ~n–S paleostress trends in the older rocks and also the related faults/brittle shears, the strain might have localized toward W. Thus, stress reoriented possibly both in space and time. The faults/brittle shears in younger Formations due S trend ~nE. Since dykes intrude faults/brittle shear planes, they swing across the 19°n latitude.

The paleostresses (~nE–nnWoriented SH_{min}) we derived are as expected for strike-slip faults (Hippolyte and Mann 2011 for Caribbean/S america strike-slip segment; Delvaux et al. 2012 for the Rukwa rift, africa). Faults may form along more than one trend (angelier 1979, 1984 and 1989). The paleostress inversion programs statistically find one single solution for all those faults considering them cogenetic. If there are separate phases of deformation, they must be clustered prior to inversion either from field criteria (liesa and lisle 2004) or statistically by some program (nemčok and lisle 1995). So, large population of faults of varying trends of one deformation event is inverted to find the orientations of the stress vectors. The parameter R can define constrictional ($\infty > R > 1$) and flattening ($1 > R > 0$) deformations. In this study area, Φ ranges 0–1 with a weak spatial pattern (Table 2; Fig. 17). The stress ratio (Φ) toward the coastal areas is lesser (≤ 0.5) than those (> 0.5) landwards. a few low magnitudes of Φ were also found at landward side. Further studies are required to analyze Φ more effectively. For an anisotropic rock with fractures/joints, faulting occurs along planes that enjoyed the greatest shear stress. attitudes of planes of preexisting anisotropies can be determined by those faults that plot between the Coulomb failure criterion and the zero-cohesion line in the Mohr diagram (Ranalli and Yin 1990; Morley et al. 2004). Reactivated faults in our terrain may be present, but we did not find any good example of superposed slickensides (similar to nickelsen 2009). However, at Kharghar (see Fig. 2 for location), we found a fault plane with sub-horizontal and sub-vertical striae (photographs with authors), but those did not superpose. Thus whether the isostatic faults predated or were coeval to strike-slip faults is difficult to ascertain. We do recognize a swing of the dykes and faults/shears, and so also the stress tensor from either n to S and E to W and/or through time. If the stress vector re-oriented temporally, the already developed structures would also do so. This needs further study. The trends of the vertical faults found in this study match the West Coast fault and the Koyna fault zone. The vertical dip-slip faults may be the surface expressions of the West Coast fault, along which the West Coast passive margin subsided (Chandrasekharam 1985; Biswas 1987; Dessai and Bertrand 1995; Sheth 1998). On the other hand, the vertical strike-slip faults reported in this study may be a northward continuation of the Koyna fault zone.

Following Morley et al. (2004), paleostress analyses of strike-slip deformations are not clear-cut since (1) the stress field may rotate temporally; (2) local features such as basement blocks and fault tips may relocate stress axes; (3) variation in the ratio of the intermediate principal stress axis with respect to the other two principal stress axes; and (4) change in failure criterion during deformation. Stress tensor calculations presume rocks to be isotropic. But most commonly rocks are anisotropic: they may contain layers and/or fractures. Only cohesive strength is to be overcome for faulting/shearing in case of pre-fractured rocks. The frictional resistance to sliding between the blocks is to be crossed for the new deformation (Davis et al. 2012). So, the pre-existing fractures/faults are easiest to reactivate than the intact isotropic rocks. Preexisting anisotropies and their reactivations may influence fault trends and therefore the paleostress tensors (Bellahsen and Daniel 2005).

Recent studies (Misra et al. 2013) reveal that the earliest opening vectors at magnetic chron C31–C30 (68–66 Ma) for the western Indian passive margin were ~nnW–SSE. Those vectors reorganized to ~nE–SW after chron C28 (63.4 Ma). These opening vectors do not conform completely with the stress tensors obtained from this study. This could be by reactivation of preexisting structures. The

vertical dip-slip (possibly isostatic) faults formed probably just after volcanism inherited the nnW–SSE western Dhar - war trend (Fig. 1). notice that the basement rock of the Deccan lavas is the Dharwar Supergroup (Ray et al. 2008; Rao et al. 2013; Roy et al. 2013). The Dharwar craton fabrics stabilized at ~3,300–2,500 Ma (Chadwick et al. 2003) much before the Deccan lava emplaced at ~68–60 Ma (Chenet et al. 2007; Ray et al. 2014). Faults/shears tend to parallel preexisting anisotropies in general, such as the foliation trends in basement (Misra and Mukherjee 2013's reviews). Subsequently, those vertical dip-slip faults with broad nW or nE trends reactivated as strike-slip faults and some new faults formed. We do not observe reactivation on faults in terms of stretching lineations of different attitudes. The lineations developed on the vertical fault planes by later strike-slip movement might had obliterated lineations of previous brittle dip-slip. This renders difficulty to separate the reactivated faults from those slipped only once. Further studies on tectonic inheritance through analogue modeling (in lines of Dooley and McClay 1997; Bellahsen et al. 2006; autin et al. 2010; see Misra and Mukherjee 2013 for reviews) and their effects in the region would reinterpret the tectonics.

We encountered no fault-related gouge, cataclasites, pseudotachylites, etc. Therefore, dating this regional strike-slip shear will not be easy. The dyke–shear relations can give merely a relative age estimate. The ~n–S to nE–SW trending Group II (~65 Ma) and Group III (~64 Ma) dykes of Hooper et al. (2010) are either strongly oriented along the shear zones or crosscut the preexisting shear zones (Fig. 15). This proves that the deformation (thus Indian–Seychelles rifting) started before these 64- to 65-Ma-old dykes emplaced. This may be as early as 80 Ma and continued till the onset of India–Seychelles breakup at ~63.4 Ma. But the precise duration of rifting is not easy to estimate since pre-rift and syn-rift rocks are difficult to obtain for dating.

The resolved paleostress tensors provide an insight of the tectonics of the India–Seychelles breakup and that it was not an orthogonal rift under E–W extension. Rather, it was a sheared margin where voluminous volcanics emplaced prior to breakup. Interestingly, Subrahmanyam and Chand (2006) also indicated oblique rifting from southernmost tip of India up to ~Mumbai (their Fig. 4) from their geophysical data. GPS measurements estimated present-day stresses (Reddy et al. 2000; Jade 2004). These studies revealed a nE–SW-trending stress: extensional near the coast and elsewhere compressional (Reddy et al. 2000). The compressional stress has been explained by the India–Eurasia collision and the coastal extensional stress possibly by unequal isostatic uplift between crustal blocks (Reddy et al. 2000). The sub-vertical dip-slip faults we encountered may be still active or rejuvenated due to loading/unloading and contribute to the present-day stress field measured in these GPS studies. Strike-slip faults and brittle shears we found do not contribute to that. Their nnW-, nE-, and E-trending extension directions (fig. 4 of Reddy et al. 2000) do not match with ours at specific locations. Pseudotachilites and/or granular injections are indicators seismic nature of faults (Stünitz et al. 2010; Rowe et al. 2012) and thus their absence in the faults we encountered in the field indicates that those were aseismic. Hence, the present-day SH_{min} from GPS measurements would not match those derived from the faults in this study. also, following Kale and Shejwalkar (2008), there is little or no present-day tectonism as understood from geomorphic evidences.

Evidences for strike-slip faulting were supported by offshore data as well. For example, fault maps by Verma et al. (2001) and naik et al. (2006) indicated strike-slip faulting. The rectangle numbered "2" in Fig. 18 shows a horsetail structure in arabian Sea in the Mumbai shelf area. Horsetail structures typify strike-slip settings (Fossen 2010; Davis et al. 2012). Here, the main fault trends nE–SW and the splay faults of the tail trend nnW–SSE to n–S (Fig. 18). The faults bounding Bombay High (Fig. 18) also resemble strike fault architecture. The usual fault patterns in orthogonal rifted basins, e.g., arcuate low dipping normal faults with relay ramps and transfer zones, are not observed here. Rather, the fault patterns match those of transtensional pull-apart basins (Dooley and McClay 1997). The Mumbai shelf region comprises of confined basins with sediments of lacustrine facies (Gopala Rao 1990), which indicates transtensional pull-apart basins. Features of transpressions could be local, but is subject to further studies (see Fossen and Tikoff 1998 for detail analyses). Seismic reflection profiles (Verma et al. 2001; naik et al. 2006) and seismogeologic cross-sections (Basu et al. 1980; Roychoudhury and Deshpande 1982; Gopala Rao 1990) neither show low-angle normal fault nor listric faulting in this region (also see Tewari 2008). Rather, all faults are sub-vertical (dip > 80°) with varying trends. Vertical faults are neither normal nor reverse, but can be strike-/dip-slip. Strike-slip faulting is likely since the fault map shows the pattern of a pull-apart basin (Fig. 18). Dip-slip faults, if present, are related to vertical adjustments (Campanile et al. 2008; Calvès et al. 2008). But since oblique-slip shear senses cannot be studied from 2D data, the offshore areas require detailed studies on 3D seismic data to quantify the deformation and resolve paleostress tensors (as in van Gent et al. 2010).

The magnetic anomalies in the northern arabian Sea adjoining the present study area can be divided into two zones: (1) where there are seafloor spreading anomalies clearly imaged and (2) where there are localized subcircular magnetic high and lows (fig. 2 of Calvès et al. 2011; Fig. 19 in this paper). Figure 19 represents the

magnetic anomalies interpreted by various authors (Bhattacharya et al. 1994; Chaubey et al. 1998; Dyment 1998; Miles et al. 1998; Todal and Edholm 1998; Collier et al. 2008). The anomalies mapped S and W of laxmi Ridge (location in Figs. 1, 20) by them are unanimous. These anomalies imply that the Indian–Seychelles plate movement was ~nE–SW (for ~nW–SE-trending magnetic chrons C30n to C27n). Then, the plate movement got ~n–S reoriented as understood from ~E–W magnetic anomaly stripes from chrons C26n to C24n and younger (Fig. 19). But those in the laxmi Basin differs in Bhattacharya et al.'s (1994) and Todal and Edholm's (1998) interpretation. The former represents an E–W extension, whereas the latter a nE–SW one. Our field evidences indicate oblique rifting, and we favor the magnetic anomaly interpretation by Todal and Edholm (1998). Recently, Misra et al. (2013) also demonstrated from a number of geophysical analyses that the extension was indeed oblique. They interpreted a ~nnW-trending plate movement vectors for chrons C31–C30 for the earliest seafloor spreading anomalies. This matches the paleostress tensors this study deciphered. Misra et al. (2013) also interpreted a second phase of ~nE-trending plate movement vectors during chrons C30–C27 (Fig. 19). This matches with those of Todal and Edholm (1998). Thus, a polyphase deformation is also indicated. Figure 20 shows the position of India–Seychelles bank and Madagascar at 70–65 Ma, i.e., just before breakup. Going with the deciphered plate movement vectors, the separation must be oblique. The obliquity could be ~40–50° as indicated by trends of the magnetic anomalies in the laxmi Basin (Fig. 19). Taken together, availability of only strike-slip deformation on sub-vertical faults/shear zones sub-parallel to the continental margin, the absence of low-angle normal faults, and SH_{min} orientations at low angles to the margin negate orthogonal rifting.

We have not tried to explain the complex tectonics of the entire west coast, which will be difficult from this study. nor did we deal with the Madagascar–India separation, which might require separate study along the entire Indian west coast. We studied and confined ourselves to the Mumbai region to explain the Seyshelles–India tectonics, since Seychelles justaposed this area before breakup (Ganerød et al. 2011). The Bombay High has been considered as a separate continental block (Bastia et al. 2010; Reeves 2013a, b). It would, in that case, become a "continental ribbon" (see Péron-Pinvidic and Manatschal 2010). But to prove as a ribbon, good seismic imaging beneath the basalts in the Mumbai shelf is needed. Since such data are unavailable, we avoid to comment.

We analyzed in detail the deformation pattern in the western Deccan basalts and accumulated a large data set for paleostress analyses. We consider that the present data can be enriched by ground-penetrating radar (GPR) surveys on the sediment-covered regions in the study area to detect the blind faults/shear zones and will result in a better understanding. This urges detailed study of the deformation along the entire western continental margin of India encompassing the states Gujarat, rest of Maharashtra, Goa, Karnataka, and Kerala. The n part of the W coast passive margin of India is a magma-rich/magmatic passive margin, which rifted obliquely. Studies on this margin with the perspective of deformation and seafloor spreading in the northern arabian Sea will establish the relationship between magma emplacement and rifting.

Key takeaways

1. Magmatism at lIPs usually does not occur after significant thinning of the crust (also see Ray et al. 2014). Bulk volcanism predated breakup. Post-volcanic deformation is evident.
2. This study goes from outcrop to regional scale through remote sensing studies into plate scale by means of Mumbai shelf fault maps and seafloor spreading anomalies to comment E–W extension to be unlikely. It is rather a ~nE–SW to ~nnW–SSE extension that separated India from Seychelles. It also matches with the deciphered plate movement vectors, though a polyphase deformation is also possible. Reactivation of vertical faults and/or reorganization of far-field stresses could be the possible results. Geodynamics of the DlIP is to be attempted.

Acknowledgments This study is a part of aaM's doctoral thesis funded by IIT Bombay. a part of the work also comes from GB's M.Sc. thesis. Sourav Sarkar, Rajkumar Ghosh, Rakesh Yadav, Rahul Biswas and Kartick Dey assisted many fieldworks. Session conveners Francesco Storti and Susanne Buiter allowed SM to present this research at the EGU, Vienna 2013. Jure Žalohar provided the license for his software T-TECTO 3.0 Professional and conversed patiently on all the programme-related queries. Discussions with Deepak Chandra Srivastava, Michal nemčok, Saibal Gupta, amit Kumar Sen, nishikanta Kundu, Roberto Weinberg, loyc Vanderkluysen, nilanjan Chatterjee, Mainak Choudhuri, Sudipta Tapan Sinha, Gn Jadhav, Tuhin Biswas, Dripta Dutta, Sidhartha Bhattacharyya and Haakon Fossen were fruitful. anindya Ghosh's comments on remote sensing were beneficial. Comments by George Mathew and especially Hetu Sheth clarified the text. This work improved immensely by three rounds very detailed external reviews by alexandre Kounov, Colin Reeves, Morgan Ganerød, and nicolas Bellahsen. We are also grateful to Global land Cover Facility (GlCF—a University of Maryland and naSa consortium) for providing the ETM + satellite data (http://glcf.umd.edu/). Thanks to Pundarika Rao for preparing the ETM + FCC images in Figs. 12 & 13. Editorial handling: Claudio Rosenberg, Wolf-Christian Dullo, Monika Dullo, nithiya Sivaraman and Springer Correction Team (Chennai).

Appendix 1

The Coulomb–navier's fracture theory states that for an isotropic rock, the fault geometry is controlled by (1) magnitudes and orientations of the principal stresses, and (2) internal friction of the rock, as per:

$$\alpha = \pm(45^\circ - \varphi/2) \quad (1)$$

where α: angle between the fracture and the maximum principal compressive stress axis; φ: angle of internal friction of the rock. Thus, σ_1 makes 30° angle with the fault for a rock with $\varphi = 30°$ and σ_3 60° for the same rock. For isotropic rocks, φ ranges 25–35°. We used this simple fracture criterion to indicate the possible σ_3 axis on the satellite images. as commonly documented in field, vertical *Y*- and *P*-planes and horizontal slip were considered.

Appendix 2

See Žalohar and Vrabec (2007) for details.

I. *s:* Dispersion parameter for the distribution of the angular misfits between the predicted and the actual direction of movement along the faults.
II. *Δ:* Threshold for the value of the compatibility measure for a fault-slip datum to be compatible with a given stress/strain.
III. q_1: approximate angle of internal friction for an intact rock. It is the slope of the tangent of the largest Mohr circle on the Mohr diagram.
IV. q_2: For a preexisting fault, it is the angle of residual friction for sliding. The parameters q_1 and q_2 constrain the possible values of the ratio between the normal and shear stress on the faults so that mechanically acceptable solutions of the inverse problem are calculated.
V. *Misfit angle:* angle between the predicted and the actual direction of slip on a fault plane. Determined by misfit functions. These functions differ with users. Žalohar and Vrabec (2007) used a Gaussian distribution function to estimate the misfit angle. Célérier et al. (2012) detailed misfit criteria and functions of previous authors.

References

allègre CJ, Birck Jl, Capmas F et al (1999) age of the Deccan traps using ^{187}Re–^{187}Os systematics. Earth Planet Sci lett 170:197–204

anderson EM (1951) The dynamics of faulting and dyke formation with special applications to Britain, 2nd edn. Oliver and Boyd, Edinburgh, p 206

angelier J (1979) Determination of the mean principal directions of stresses for a given fault population. Tectonophysics 56:T17–T26

angelier J (1984) Tectonic analysis of fault slip data sets. J Geophys Res Solid Earth 89:5835–5848

angelier J (1989) From orientation to magnitudes in paleostress determinations using fault slip data. J Struct Geol 11:37–50

angelier J (1994) Fault slip analysis and palaeostress reconstruction. In: Hancock Pl (ed) Continental deformation. Pergamon Press, Oxford, pp 53–100

angelier J, Mechler P (1977) a graphic method applied to the localization of principal stresses for fault tectonics and seismology: the right dihedral method. Bull Soc Geol Fr 19:1309–1318

angelier J, Bergerat F, Chu HT et al (1990) Paleostress analysis as a key to margin extension: the Penghu Islands, South China Sea. Tectonophysics 183:161–176

armijo R, Cisternas a (1978) Un problème inverse en microtectonique cassante. C R acad Sci D287:595–598

armitage JJ, Collier JS, Minshull T a et al (2011) Thin oceanic crust and flood basalts: India–Seychelles breakup. Geochem Geophys Geosyst 12:Q0aB07

auden JB (1949) Dykes in western India—a discussion of their relationships with the Deccan Trap. Trans natl Inst Sci Ind 3:13–157

autin J, Bellahsen n, Husson l et al (2010) analog models of oblique rifting in a cold lithosphere. Tectonics 29:TC6016

a ydin a, DeGraff JM (1988) Evolution of polygonal fracture patterns in lava flows. Science 239:471–476

azeez KKa, Kumar TS, Basava S et al (2011) Hydrocarbon prospects across narmada–Tapti rift in Deccan trap, central India: inferences from integrated interpretation of magnetotelluric and geochemical prospecting studies. Mar Pet Geol 28:1073–1082

Babar M, Chunchekar R, Yadava MG, Ghute B (2012) Quaternary geology and geomorphology of Terna River Basin in west central India. Quat Sci J 61:156–167

Babechuk MG, Widdowson M, Kamber BS (2014) Quantifying chemical weathering intensity and trace element release from two contrasting basalt profiles, Deccan Traps. India Chem Geol 363:56–75

Baksi aK, Farrar E (1991) ^{40}ar/ ^{39}ar dating of the Siberian Traps, USSR: evaluation of the ages of the two major extinction events relative to episodes of flood-basalt volcanism in the USSR and Deccan Traps, India. Geology 19:461–464

Balasubrahmanyan Mn (2006) Geology and tectonics of India: an overview, Chapter 10. Ia GR Mem no. 9, pp 125–130

Bastia R, Reeves C, Pundarika Rao D et al (2010) Paleogeographic reconstruction of East Gondwana and evolution of the Indian continental margin. DCS-DST news august 2–8

Basu Dn, Banerjee a, Tamhane DM (1980) Source areas and migration trends of oil and gas in Bombay Offshore Basin, India. am assoc Pet Geol Bull 64:209–220

Beane J, Turner C, Hooper P et al (1986) Stratigraphy, composition and form of the Deccan basalts, Western Ghats, India. Bull Volcanol 48:61–83

Becker J, Sandwell D, Smith W et al (2009) Global bathymetry and elevation data at 30 arc seconds resolution: SRTM30_PlUS. Mar Geod 32:355–371

Bellahsen n, Daniel JM (2005) Fault reactivation control on normal fault growth: an experimental study. J Struct Geol 27:769–780

Bellahsen n, Fournier M, d'acremont E, et al (2006) Fault reactivation and rift localization: northeastern Gulf of aden margin. Tectonics 25:TC1007

Berthé D, Choukroune P, Jegouzo P (1979) Orthogneiss, mylonite and non-coaxial deformation of granite: the example of the south armorican shear zone. J Struct Geol 1:31–42

Bhattacharji S, Chatterjee n, Wampler JM et al (1996) Indian intraplate and continental margin rifting, lithospheric extension, and mantle upwelling in Deccan flood basalt volcanism near the K/T boundary: evidence from Mafic Dike Swarms. J Geol 104:379–398

Bhattacharya G (2013) The volcanic mesas of western Deccan, India. Geol Today 29:168

Bhattacharya G, Chaubey a, Murty G et al (1994) Evidence for seafloor spreading in the laxmi Basin, northeastern arabian Sea. Earth Planet Sci lett 125:211–220

Biswas SK (1987) Regional tectonic framework, structure and evolution of the western marginal basins of India. Tectonophysics 135:307–327

Bondre n, Hart W, Sheth H (2006) Geology and geochemistry of the Sangamner mafic dike swarm, western Deccan volcanic province, India: implications for regional stratigraphy. J Geol 114:155–170

Bott MHP (1959) The mechanics of oblique slip faulting. Geol Mag 96:109–117

Brahmam nK, negi JG (1973) Rift valleys beneath Deccan Traps (India). Geophys Res Bull 11:207

Calvès G, Clift PD, Inam a (2008) anomalous subsidence on the rifted volcanic margin of Pakistan: no influence from Deccan plume. Earth Planet Sci lett 272:231–239

Calvès G, Schwab aM, Huuse M et al (2011) Seismic volcanostratigraphy of the western Indian rifted margin: the pre-Deccan igneous province. J Geophys Res Solid Earth 116:B01101

Campanile D (2007) The post-breakup evolution of the western Indian high-elevation passive margin. University of Glasgow, PhD thesis, pp 1–210

Campanile D, nambiar CG, Bishop P et al (2008) Sedimentation record in the Konkan–Kerala Basin: implications for the evolution of the Western Ghats and the Western Indian passive margin. Basin Res 20:3–22

Caputo R (1995) Evolution of orthogonal sets of coeval extension joints. Terra nova 7:479–490

Caputo R (2010) Why joints are more abundant than faults. a conceptual model to estimate their ratio in layered carbonate rocks. J Struct Geol 32:1257–1270

Carey E, Brunier B (1974) analyse théorique et numérique d'une modeèle méchanique élémentaire appliqué a l'étude d'une population de failles. C R acad Sci D 279:891–894

Cater FW (1982) Intrusive rocks of the Holden and lucerne Quadrangle, Washington—the relation of depth zones, composition, textures and emplacement of plutons. Geol Surv Prof Pap 1220:86

Célérier B, Etchecopar a, Bergerat F et al (2012) Inferring stress from faulting: from early concepts to inverse methods. Tectonophysics 581:206–219

Chadwick B, Vasudedev Vn, Hegde GV (2003) Chitradurga Schist Belt and its adjacent Plutonic Rocks, nW of Tungabhadra, Karnataka: a duplex in the late archaean convergent setting of the Dharwar Craton. J Geol Soc India 61:645–663

Chalapathy Rao n, lehmann B (2011) Kimberlites, flood basalts and mantle plumes: new insights from the Deccan large igneous province. Earth-Sci Rev 107:315–324

Chandrasekhar P, Martha TR, Venkateswarlu n et al (2011) Regional geological studies over parts of Deccan Syneclise using remote sensing and geophysical data for understanding hydrocarbon prospects. Curr Sci 100:95–99

Chandrasekharam D (1985) Structure and evolution of the western continental margin of India deduced from gravity, seismic, geomagnetic and geochronological studies. Phys Earth Planet Int 41:186–198

Chaubey a, Bhattacharya G, Murty G et al (1998) Early Tertiary seafloor spreading magnetic anomalies and paleo-propagators in the northern arabian Sea. Earth Planet Sci lett 154:41–52

Chaubey aK, Gopala Rao D, Srinivas K et al (2002) analyses of multichannel seismic reflection, gravity and magnetic data along a regional profile across the Central-Western Continental Margin of India. Mar Geol 182:303–323

Chen Y, Jiang D, Zhu G (2014) The formation of micafish: a modeling investigation based on micromechanics. J Struct Geol. doi:10.1016/j.jsg.2013.12.005

Chenet a, Quidelleur X, Fluteau F et al (2007) 40K–40ar dating of the main Deccan large igneous province: further evidence of KTB age and short duration. Earth Planet Sci lett 263:1–15

Ciancaleoni l, Marquer D (2006) Syn-extension leucogranite defor - mation during convergence in the eastern central alps: example of the novate intrusion. Terra nova 18:170–180

Collier J, Sansom V, Ishizuka O et al (2008) age of Seychelles–India break-up. Earth Planet Sci lett 272:264–277

Collier JS, Minshull Ta, Hammond JOS et al (2009) Factors controlling the degree of magmatism during continental breakup: new insights from a wide-angle seismic experiment across the conjugate Seychelles–Indian margins. J Geophys Res Solid Earth 114:B03101

Correa-Gomes lC, Souza Filho CR, Martins CJFn et al (2001) Development of symmetrical and asymmetrical fabrics in sheet-like igneous bodies: the role of magma flow and wall-rock displacements in theoretical and natural cases. J Struct Geol 23:1415–1428

Courtillot V, Besse J, Vandamme D et al (1986) Deccan flood basalts at the Cretaceous/Tertiary boundary? Earth Planet Sci lett 80:361–374

Courtillot V, Feraud G, Maluski H et al (1988) Deccan flood basalts and the Cretaceous/Tertiary boundary. nature 333:843–846

Courtillot V, Jaupart C, Manighetti I et al (1999) On causal links between flood basalts and continental breakup. Earth Planet Sci lett 166:177–195

Courtillot V, Gallet Y, Rocchia R et al (2000) Cosmic markers, ^{40}ar/ ^{39}ar dating and paleomagnetism of the KT sections in the anjar area of the Deccan large igneous province. Earth Planet Sci lett 182:137–156

Cox KG, Hawkesworth CJ (1984) Relative contribution of crust and mantle to flood basalt volcanism, Mahabaleshwar area, Deccan Traps. Philos Trans R Soc lond 310:627–641

Creixell C, Parada MÁ, Roperch P et al (2006) Syntectonic emplacement of the Middle Jurassic Concón Mafic Dike Swarm, Coastal Range, central Chile (33° S). Tectonophysics 425:101–122

Cripps J, Widdowson M, Spicer R et al (2005) Coastal ecosystem responses to late stage Deccan Trap volcanism: the post K–T boundary (danian) palynofacies of Mumbai (Bombay), west India. Palaeogeol Palaeoclimatol Palaeoecol 216:303–332

Datta Gupta S, Chatterjee R, Farooqui MY (2012) Formation evaluation of fractured basement, Cambay Basin, India. J Geophys Eng 9. http://iopscience.iop.org/1742-2140/9/2/162/pdf/1742-2140_9_2_162.pdf. accessed on 10 Jan 2014

Davis Ga, lister GS (1988) Detachment faulting in continental extension; perspectives from the Southwestern U.S, Cordillera. Geol Soc am Spec Pap 218:133–159

Davis GH, Bump aP, García PE et al (1999) Conjugate Riedel defor - mation band shear zones. J Struct Geol 22:169–190

Davis GH, Reynolds SJ, Kluth C (2012) Structural geology of rocks and regions, 3rd edn. Wiley, new York, pp 507, 508, 541

De a (1981) late Mesozoic–lower Tertiary magma types of Kutch and Saurashtra. Mem Geol Soc India 3:327–339

Delvaux D, Kervyn F, Macheyeki aS et al (2012) Geodynamic significance of the TRM segment in the East african Rift (W-Tanzania): active tectonics and paleostress in the Ufipa plateau and Rukwa basin. J Struct Geol 37:161–180

Deshmukh SS, Sehgal Mn (1988) Mafic dyke swarms in Deccan Volcanic Province of Madhya Pradesh and Maharashtra. Mem Geol Soc India 10:323–340

Deshpande GG (1998) Geology of Maharashtra. Geol Soc India, Bangalore

Dessai a, Bertrand H (1995) The “Panvel flexure” along the western Indian continental margin: an extensional fault structure related to Deccan magmatism. Tectonophysics 241:165–178

Dessai a, Bodas MS (1984) Occurrence of nepheline Syenite around Murud–Janjira Raigarh District, Maharashtra, India. Curr Sci 53:775–777

Dessai a, Viegas a (1995) Multi-generation mafic dyke swarm related to Deccan magmatism, south of Bombay: implications on the evolution of the western Indian continental margin. Mem Geol Soc India 47:435–451

Destro n, Szatmari P, alkmim FF et al (2003) Release faults, associated structures, and their control on petroleum trends in the Recôncavo Rift, northeast Brazil. am assoc Pet Geol Bul 87:1123–1144

Devey CW, lightfoot P (1986) Volcanological and tectonic control of stratigraphy and structure in the western Deccan Traps. Bull Volcanol 48:195–207

Devey CW, Stephens W (1991) Tholeiitic dykes in the Seychelles and the original spatial extent of the Deccan. J Geol Soc lond 148:979–983

Devey CW, Stephens WE, (1992) Deccan related mag- matism west of the Seychelles-lndia rift. In: al-abaster BC, Pankhurst RJ (eds) Magmatism and the causes of continental break-up, vol 68. Geological Society london, Special Publication, pp 271–291

Doblas M (1998) Slickenside kinematic indicators. Tectonophysics 295:187–197

Doblas M, Faulkner D, Mahecha V et al (1997) Morphologically ductile criteria for the sense of movement on slickensides from an extensional detachment fault in southern Spain. J Struct Geol 19:1045–1054

Dole G, Peshwa VV, Kale VS (2000) Evidence of a Paleoseismic event from Deccan Plateau Uplands. J Geol Soc India 56:547–555

Dooley T, McClay K (1997) analog modeling of pull-apart basins. aaPG Bull 81:1804–1826

Duncan Ra (1990) The volcanic record of the rèunion hotspot, In: Duncan Ra, Backman J, Peterson lC et al (eds) Proc Ocean Drill Prog Sci Res 115, pp 3–10

Duncan Ra, Storey M (1992) The life cycle of Indian Ocean hot spots. In: Duncan Ra (ed) Synthesis of results from scientific drilling in the Indian Ocean. am Geophys Univ Geophys Monogr 70, pp 91–103

Duraiswami Ra, Das S, Shaikh Tn (2012) Hydrogeological framework of aquifers in the Deccan Traps, India: some insights. In: Pawar nJ, Das S, Duraiswami Ra (eds) Hydrogeology of Deccan Traps and associated formations in Penninsular India. Geol Soc India, Bangalore

Dyment J (1998) Evolution of the Carlsberg Ridge between 60 and 45 Ma: ridge propagation, spreading asymmetry, and the Deccan–Rèunion hotspot. J Geophys Res Solid Earth 103:24067–24084

Dzulynski S, Kotlarczyk J (1965) Tectogliphs on slickensided surfaces. Bull Pol acad Sci 13:149–154

Eig K, Bergh SG (2011) late Cretaceous–Cenozoic fracturing in lofoten, north norway: tectonic significance, fracture mechanisms and controlling factors. Tectonophysics 499:190–205

Etchecopar a, Vasseur G, Daignieres M (1981) an inverse problem in microtectonics for the determination of stress tensors from fault striation analysis. J Struct Geol 3:51–65

Fossen H (2010) Structural geology. Cambridge University Press, Cambridge, pp 124, 135, 191, 198, 463

Fossen H, Tikoff B (1998) Extended models of transpression and transtension, and application to tectonic settings. In: Holdsworth RE, Strachan Ra, Dewey JE (eds) Continental transpressional and transtensional tectonics. Geol Soc lond Spec Publ 135, pp 15–33

Fowler CMR (2005) The solid earth: an introduction to global geophysics. Cambridge University Press, Cambridge, pp 567–577

Ganerød M (2010) Geochronology and paleomagnetism of large Igneous Provinces, the north atlantic Igneous Province and the Deccan Traps. PhD Thesis, norwegian University of Science and Technology, Trondheim. http://www.geodynamics.no/people/morgan.html. a vailed on 09 Jan 2014

Ganerød M, Torsvik T, van Hinsbergen D et al. (2011) Palaeoposition of the Seychelles microcontinent in relation to the Deccan traps and the plume generation zone in late Cretaceous–early Palaeogene time. In: van Hinsbergen DJJ, Buiter SJH, Torsvik TH et al (eds) The formation and evolution of africa: a synopsis of 3.8 Ga of earth history. Geol Soc lond Spec Publ 357, pp 229–252

Glazner a, Bartley J, Carl B (1999) Oblique opening and noncoaxial emplacement of the Jurassic independence dike swarm, California. J Struct Geol 21:1275–1283

Godbole S, Rana R, natu S (1996) lava stratigraphy of Deccan basalts of western Maharashtra. Gondwana Geol Mag Spec Publ 2:125–134

Gombos aM, Powell WG, norton IO (1995) The tectonic evolution of western India and its impact on hydrocarbon occurrences—an overview. Sediment Geol 96:119–129

Gopala Rao D (1990) Magnetic studies of basement off the coast of Bombay, west of India. Tectonophysics 175:317–334

Gudmundsson a (1984) Formation of dykes, feeder-dykes, and the intrusion of dykes from magma chambers. Bull Volcanol 47:537–550

Gudmundsson a (2011) Rock fractures in geological processes. Cambridge University Press, new York, pp 327–340

Guha SK, Padale JG (1981) Seismicity and structure of the Deccan Trap region. In: Subbarao KV, Sukeshwala Rn (eds) Deccan volcanism and related basalt provinces in other parts of the world. Geol Soc Ind Mem no. 3, Bangalore, pp 153–164

Guidi GD, Caputo R, Scudero S (2013) Regional and local stress field orientation inferred from quantitative analyses of extension joints: case study from southern Italy. Tectonics 32:239–251

Gupta HK, Rao RUM, Srinivasa R et al (1999) anatomy of sur - face rupture zones of two stable continental region earthquakes, 1967 Koyna and 1993 latur, India. Geophys Res lett 26:1985–1988

Hancock P (1985) Brittle microtectonics: principles and practice. J Struct Geol 7:437–457

Hargraves RB, Duncan Ra (1990) Radiometric age and paleomagnetic results from Seychelles dikes. In: Duncan Ra, Backman J, Peterson lC et al (eds) Proc ODP Sci Results 115. College Station, TX (Ocean Drilling Program), pp 119–122

Harinarayana T, Patro BPK, Veeraswamy K et al (2007) Regional geoelectric structure beneath Deccan Volcanic Province of the Indian subcontinent using magnetotellurics. Tectonophysics 445:66–80

Herman GC (2009) Steeply-dipping extension fractures in the newark basin, new Jersey. J Struct Geol 31:996–1011

Hippolyte JC, Mann P (2011) neogene–Quaternary tectonic evolution of the leeward antilles islands (aruba, Bonaire, Curaçao) from fault kinematic analysis. Mar Pet Geol 28:259–277

Hodgson Ra (1961) Regional study of jointing in Comb Ridge-navajo mountain area, arizona and Utah. aaPG Bull 45:1–38

Hofmann C, Féraud G, Courtillot V (2000) ^{40}ar/ ^{39}ar dating of mineral separates and whole rocks from the Western Ghats lava pile: further constraints on duration and age of the Deccan traps. Earth Planet Sci lett 180:13–27

Hooper PR (1990) The timing of crustal extension and the eruption of continental flood basalts. nature 345:246–249

Hooper P, Widdowson M, Kelley S (2010) Tectonic setting and timing of the final Deccan flood basalt eruptions. Geology 38:839–842
Hutton D (1992) Granite sheeted complexes: evidence for the dyking ascent mechanism. Trans R Soc Edinb Earth Sci 83:377–382
Jade S (2004) Estimates of plate velocity and crustal deformation in the Indian subcontinent using GPS geodesy. Curr Sci 86:1443–1448
Jain PK, Gupta DC (2013) Geochemistry of intrusive rocks of Deccan Trap region around Manmad, nasik, India. Int J adv Earth Environ Sci 1:1–13
Jayaraman K (2007) India's carbon dioxide trap. nat Geosci 445:350
Jones RMP (1980) Basinal isostatic adjustment faults and their petroleum significance. Bull Can Pet Geol 28:211–251
Ju W, Hou G, Hari K (2013) Mechanics of mafic dyke swarms in the Deccan large igneous province: palaeostress field modelling. J Geodyn 66:79–91
Kaila Kl, Reddy PR, Dixit MM et al (1981) Deep crustal structure at Koyna, Maharashtra indicated by deep seismic profiling. J Geol Soc India 22:1–16
Kailasam l (1975) Epeirogenic studies in India with reference to recent vertical movements. Tectonophysics 29:505–521
Kailasam l (1979) Plateau uplift in peninsular India. Tectonophysics 61:243–269
Kale VS, Peshwa VV (1995) The Bhima Basin. Geol Soc India, Bangalore, p 142
KaleVS Shejwalkar n (2008) Uplift along the western margin of the Deccan Basalt Province: is there any geomorphometric evidence? J Earth Syst Sci 117:959–971
Kaplay RD, Vijay Kumar T, Sawant R (2013) Field evidence for deformation in Deccan Traps in microseismically active nanded area, Maharashtra. Curr Sci 105:1051–1052
Katz Y, Weinberger R, a ydin a (2004) Geometry and kinematic evolution of Riedel shear structures, Capitol Reef national Park, Utah. J Struct Geol 26:491–501
Kaven J, Maerten F, Pollard D (2011) Mechanical analysis of fault slip data: implications for paleostress analysis. J Struct Geol 33:78–91
Keary P, Klepsis Ka, Vine FJ (2009) Global tectonics, 3rd edn. Wiley, Sussex, p 482
Klausen MB, larsen HC (2002) East Greenland coast-parallel dike swarm and its role in continental breakup. In: Menzies Ma, Klemperer Sl, Ebinger CJ, Baker J (eds) Volcanic rifted mar - gins. Geol Soc am Spec Pap 362, pp 133–158
Knight KB, Renne PR, Halkett a et al (2003) ^{40}ar/ ^{39}ar dating of the Rajahmundry Traps, eastern India and their relationship to the Deccan traps. Earth Planet Sci lett 208:85–99
Kolla V, Coumes F (1990) Extension of structural and tectonic trends from the Indian subcontinent into the eastern arabian Sea. Mar Pet Geol 7:188–196
Koyi Ha, Schmeling H, Burchardt S et al (2013) Shear zones between rock units with no relative movements. J Struct Geol 50:82–90
Kranis H (2007) neotectonic basin evolution in central-eastern mainland Greece: an overview. Bull Geol Soc Greece 40:360–373
Kraus S, Poblete F, arriagada C (2010) Dike systems and their volcanic host rocks on King George Island, antarctica: implications on the geodynamic history based on a multidisciplinary approach. Tectonophysics 495:269–297
Kumar P, Yuan X, Kumar MR et al (2007) The rapid drift of the Indian tectonic plate. nature 449:894–897
Kumar D, Thiagarajan S, Rai Sn (2011) Deciphering geothermal resources in Deccan trap region using electrical resistivity tomography technique. J Geol Soc India 78:541–548
Kundu B, Matam a (2000) Identification of probable faults in the vicinity of Harnai–Ratnagiri region of the Konkan coast, Maharashtra, India. Curr Sci 78:1556–1560
lacombe O (2012) Do fault slip data inversions actually yield "paleostresses" that can be compared with contemporary stresses? a critical discussion. C R Geosci 344:159–173
lescinsky DT, Fink JH (2000) lava and ice interaction at stratovolcanoes: use of characteristic features to determine past glacial extents and future volcanic hazards. J Geophys Res Solid Earth 105:23711–23726
liesa Cl, lisle RJ (2004) Reliability of methods to separate stress tensors from heterogeneous fault–slip data. J Struct Geol 26:559–572
lightfoot PC, Hawkesworth CJ, Sethna SF (1987) Petrogenesis of rhyolites and trachytes from the Deccan Traps: Sr, nd and Pb isotope and trace element evidence. Contrib Mineral Petrol 95:44–54
lisle RJ (1989) Paleostress analysis from sheared dike sets. Geol Soc am Bull 101:968–972
luther al, axen GJ, Selverstone J et al (2009) Is low angle normal fault slip by local stress rotations? assessment of paleostress inversion methods. a GU, Fall Meeting-abstract. http://adsabs.harvard.edu/abs/2009a GUFM.T41a1993l. accessed on 30 nov 2011
Mahadevan TM (1994) Deep continental structure of India. Geol Soc Ind Mem 28, Bangalore, pp 237–296, 474–476
Mahoney JJ (1988) Deccan traps. In: MacDougall JD (ed) Continental flood basalts. Kluwer, Dordrecht, pp 151–194
Mahoney JJ, Duncan Ra, Khan W et al (2002) Cretaceous volcanic rocks of the South Tethyan suture zone, Pakistan: implications for the Rèunion hotspot and Deccan Traps. Earth Planet Sci lett 203:295–310
Malavieille J (1987) Kinematics of compressional and extensional ductile shearing deformation in a metamorphic core of the northern Basin and Range. J Struct Geol 9:541–554
Maldonaldo a, Stanley DJ (1976) late Quaternary sedimentation and stratigraphy in the strait of Sicily. Smithson Contrib Earth Sci 16. http://www.sil.si.edu/smithsoniancontributions/EarthSciences/pdf_hi/sces-0016.pdf. accessed on 04 aug 2013
Malod J, Droz l, Kemal BM et al (1997) Early spreading and continental to oceanic basement transition beneath the Indus deep-sea fan: northeastern arabian Sea. Mar Geol 141:221–235
Marquer D, Challandes n, Baudin T (1996) Shear zone patterns and strain partitioning at the scale of a Penninic nappe: the Suretta nappe (Eastern Swiss alps). J Struct Geol 18:753–764
Menegon l, Pennacchioni G (2010) local shear zone pattern and bulk deformation in the Gran Paradiso metagranite (nW Italian alps). Int J Earth Sci 99:1805–1825
Menzies Ma, Klemperer Sl, Ebinger CJ et al (2002) Characteristics of volcanic rifted margins. In: Menzies Ma, Klemperer Sl, Ebinger CJ et al. (eds) Volcanic rifted margins. Geol Soc am Spec Pap 362, pp 1–14
Miggins DP, Thompson Ra, Pillmore Cl et al (2002) Extension and uplift of the northern Rio Grande Rift: evidence from 40ar/39ar geochronology from the Sangre de Cristo Mountains, south-central Colorado and northern new Mexico. In: Menzies Ma, Klemperer Sl, Ebinger CJ, et al (eds) Volcanic rifted margins. Geol Soc am Spec Pap 362, pp 47–64
Miles PR, Munschy M, Segoufin J (1998) Structure and early evolution of the arabian Sea and East Somali Basin. Geophys J Int 134:876–888
Mishra DC (2012a) Gravity and magnetic methods in geological studies: principles, integrated exploration and plate tectonics. B.S. Publications, Hyderabad
Mishra OP (2012) Seismological research in India. In: Banerjee DM, Singhvi aK (eds) Glimpses of geoscience research in India. Indian report to the IUGS: 2008–2012. Proc Ind nat Sci acad 78, pp 361–371

Mishra DC, Tiwari VM, Singh B (2008) Gravity studies in India and their Geological Significance. In: Subbarao KV, Sukeshwala Rn (eds) Deccan volcanism and related basalt provinces in other parts of the world. Geol Soc Ind Mem no. 3, Bangalore, pp 329–372

Misra aa (2014) Photograph of the month. J Struct Geol 60:105

Misra aa, Bhattacharya G (2014) Rare slickenside kinematic indicator “asymmetric Elevations” seen abundant in southern aksa Beach, Mumbai, India. Int J Earth Sci 103:327–328

Misra aa, Mukherjee S (2013) Role of tectonic inheritance in passive margin architecture: a review. Symposium in Honour of Davis Robert. Basin Dynamics and Petroleum Systems: Geophysics, Structure, Stratigraphy, Sedimentology and Geochemistry. 14–16 april 2014. Windsor Building, Royal Holloway University of london (submitted abstract)

Misra aa, Sinha n, Mukherjee S (2013) Repeat ridge jumps and microcontinent separation: insights from nE arabian Sea. Mar Pet Geol (submitted)

Mitchell C, Widdowson M (1991) a geological map of the southern Deccan Traps, India and its structural implications. J Geol Soc lond 148:495–505

Mohan G, Kumar MR (2004) Seismological constraints on the structure and composition of western Deccan volcanic province from converted phases. Geophys Res lett 31:l02601

Mohan G, Surve G, Tiwari PK (2007) Seismic evidences of faulting beneath the Panvel flexure. Curr Sci 93:991–996

Morgan WJ (1972) Deep mantle convection plumes and plate motions. aaPG Bull 56:203–213

Morley CK, Haranya C, Phoosongsee W et al (2004) activation of rift oblique and rift parallel pre-existing fabrics during extension and their effect on deformation style: examples from the rifts of Thailand. J Struct Geol 26:1083–1829

Mukherjee S (2007) Geodynamics, deformation and mathematical analysis of metamorphic belts of the nW Himalaya. Unpublished Ph.D. thesis. Indian Institute of Technology Roorkee, pp 1–267

Mukherjee S (2010a) Structures at meso and micro-scales in the Sutlej section of the Higher Himalayan shear zone in Himalaya. e-Terra 1–27

Mukherjee S (2010b) Microstructures of the Zanskar Shear Zone. Earth Sci India 3:9–27

Mukherjee S (2011) Mineral fish: their morphological classification, usefulness as shear sense indicators and genesis. Int J Earth Sci 100:1303–1314

Mukherjee S (2012a) Tectonic Implications and Morphology of Trapezoidal Mica Grains from the Sutlej Section of the Higher Himalayan Shear Zone, Indian Himalaya. J Geol 120:575–590

Mukherjee S (2012b) a micro-duplex. Int J Earth Sci 101:503

Mukherjee S (2012c) Simple shear is not so simple! Kinematics and shear senses in newtonian viscous simple shear zones. Geol Mag 149:819–826

Mukherjee S (2013a) Review of flanking structures in meso- and micro-scales. Geol Mag (in press). doi:10.1017/S0016756813001088

Mukherjee S (2013b) atlas of shear zone structures in meso-scale. Springer, Cham. ISBn 978-3-319-00088-6

Mukherjee S (2013c) Higher Himalaya in the Bhagirathi section (nW Himalaya, India): its structures, backthrusts and extrusion mechanism by both channel flow and critical taper mechanisms. Int J Earth Sci 102:1851–1870

Mukherjee S (2013d) Deformation microstructures in rocks. Springer. ISBn: 978-3-642-25607-3

Mukherjee S, Koyi Ha (2010a) Higher Himalayan Shear Zone, Sutlej section: structural geology and extrusion mechanism by various combinations of simple shear, pure shear and channel flow in shifting modes. Int J Earth Sci 99:1267–1303

Mukherjee S, Koyi Ha (2010b) Higher Himalayan Shear Zone, Zanskar Indian Himalaya—microstructural studies & extrusion mechanism by a combination of simple shear & channel flow. Int J Earth Sci 99:1083–1110

Mukhopadhyay R, Fernandes Wa, naik YS et al (2010) an insight into the “Fifty-Fathom-Flat” off India’s west coast. Geomorphology 118:465–470

Müller RD, Gaina C, Roest WR et al (2001) a recipe for microcontinent formation. Geology 29:203–206

naik G, Gandhi D, Singh a et al (2006) Paleocene-to-early Eocene tectono-stratigraphic evolution and paleogeographic reconstruction of Heera-Panna-Bassein, Bombay offshore basin. lead Edge 25:1071–1077

nemčok M, lisle RJ (1995) a stress inversion procedure for polyphase fault/slip data sets. J Struct Geol 17:1445–1453

nickelsen RP (2009) Overprinted strike-slip deformation in the southern Valley and Ridge in Pennsylvania. J Struct Geol 31:865–873

Owen-Smith TM, ashwal lD, Torsvik TH et al (2013) Seychelles alkaline suite records the culmination of Deccan Traps continental flood volcanism. lithos 182:33–47

Park S, Kim Y, Ryoo C et al (2010) Fractal analysis of the evolution of a fracture network in a granite outcrop, SE Korea. Geosci J 14:201–215

Parthasarathy a, Panchpakeshan V, nagarajan R (2013) Engineering geology. Wiley, new York, pp 382–392

Passchier CW, Trouw Ra (2005) Microtectonics, 2nd edn. Springer, Berlin, pp 157–158

Pawar nJ, Das S, Duraiswami RS (2012) Hydrogeology of Deccan Traps and associated Formations in Peninsular India. Edited volume. Geol Soc Ind Mem 80

Peng ZX, Mahoney JJ (1995) Drillhole lavas from the northwestern Deccan Traps, and the evolution of Rèunion hot spot mantle. Earth Planet Sci lett 134:169–185

Peng ZX, Mahoney JJ, Vanderkluysen l et al (2014) Sr, nd and Pb isotopic and chemical compositions of central Deccan Traps lavas and relation to southwestern Deccan stratigraphy. J asian Earth Sci 84:83–94

Péron-Pinvidic G, Manatschal G (2010) From microcontinents to extensional allochthons: witnesses of how continents rift and break apart? Pet Geosci 16:189–197

Peshwa VV, Kale VS (1988) Role of remote sensing in the detection of potential sites for landslides/rockfalls in the Deccan Trap lava terrain of western India. Environmental Geotechnics and Problematic Soils and Rocks, Balkema, Rotterdam, pp 367–374

Peshwa VV, Kale VS (1997) neotectonics of the Deccan Traps Province: focus on the Kurduwadi lineament. J Geophys 1:77–86

Peshwa VV, Mulay JG, Kale VS (1987) Fracture zones in the Deccan Traps of Western and Central India: a study based on remote sensing techniques. J Indian Soc Remote Sensing 15:9–17

Petit J (1987) Criteria for the sense of movement on fault surfaces in brittle rocks. J Struct Geol 9:597–608

Plummer PS, Belle E (1995) Mesozoic tectono-stratigraphic evolution of the Seychelles microcontinent. Sediment Geol 96:73–91

Plummer PS, Joseph PR, Samson PJ (1998) Depositional environments and oil potential of Jurassic/Cretaceous source rocks within the Seychelles microcontinent. Mar Pet Geol 15:385–401

Pollyea RM, Fairley JP, Podgorney RK (2014) Physical constraints on geologic CO2 sequestration in low-volume basalt formations. GSa Bull 126:344–351

Powar KB (1981) lineament fabric and dyke pattern in the western part of the Deccan volcanic province. In: Subbarao KV, Sukeshwala Rn (eds) Deccan Volcanism and Related Basalt Provinces in other parts of the world. Geol Soc Ind Mem no. 3. Bangalore. pp. 45-57.

Prasanna lakshmi KJ, Senthil Kumar P, Vijayakumar K et al (2014) Petrophysical properties of the Deccan basalts exposed in the

Western Ghats escarpment around Mahabaleshwar and Koyna, India. J asian Earth Sci 84:176–187
Qureshy Mn (1981) Gravity anomalies, isostasy and crust mantle relations in the Deccan trap and contiguous regions, India. In: Subbarao KV, Sukeshwala Rn (eds) Deccan volcanism and related basalt provinces in other parts of the world. Geol Soc Ind Mem no. 3, Bangalore, pp 184–197
Rai SS, Ramesh DS (2012) Seismic imaging of the Indian continental lithosphere. In: Banerjee DM, Singhvi aK (eds) Glimpses of geoscience research in India. Indian report to the IUGS: 2008–2012. Proc Indian natl Sci acad 78, pp 353–359
Rai Sn, Thiagarajan S, Kumari YR (2011) Exploration for groundwater in the basaltic Deccan traps terrain in Katol Taluk, nagpur District, India. Curr Sci 1198–1205
Ramsay JG, Huber MI (1987) The techniques of modern structural geology, vol 2: folds and fractures. academic Press, london, pp 529–530
Ranalli G, Yin ZM (1990) Critical stress difference and orientation of faults in rocks with strength anisotropies: the two-dimensional case. J Struct Geol 12:1067–1071
Rao nP, Roy S, arora K (2013) Deep Scientific Drilling in Koyna, India—Brain-storming workshop on geological investigations 19–20, March 2013. J Geol Soc India 81:722–723
Ray R, Sheth HC, Mallik J (2007) Structure and emplacement of the nandurbar–Dhule mafic dyke swarm, Deccan Traps, and the tectonomagmatic evolution of flood basalts. Bull Volcanol 69:537–551
Ray R, Shukla aD, Sheth HC et al (2008) Highly heterogeneous Precambrian basement under the central Deccan Traps, India: direct evidence from xenoliths in dykes. Gondwana Res 13:375–385
Ray D, Misra M, Widdowson M et al (2014) a common percentage for Deccan Continental Flood Basalt and Central Indian Ocean Ridge Basalt? a Geochemical and isotopic approach. J asian Earth Sci 84:188–200
Reddy CD, El-fiky G, Kato T, et al (2000) Crustal strain field in the Deccan trap region, western India, derived from GPS measurements. Earth Planets Sp 52:965–969
Reeves CV (2013a) The global tectonics of the Indian Ocean and its relevance to India's western margin. J Geophys 34:87–94
Reeves CV (2013b) The position of Madagascar within Gondwana and its movements during Gondwana dispersal. J afr Earth Sci. doi:10.1016/j.jafrearsci.2013.07.011
Reynolds SJ, lister GS (1990) Folding of mylonitic zones in Cordilleran core complexes: evidence from near the mylonitic front. Geology 18:216–219
Richards Ma, Duncan Ra, Courtillot VE (1989) Flood basalts and hotspot tracks: plume heads and tails. Science 246:103–107
Rowe CD, Kirkpatrick JD, Brodsky EE (2012) Fault rock injections record paleo-earthquakes. Earth Planet lett 335–336:154–166
Roy aB (2012) Indian Shield: insight into the pristine size, shape and tectonic framework. Indian J Geosci 66:181–192
Roy S, Rao nP, akkiraju VV et al (2013) Granitic basement below Deccan Traps Unearthed by drilling in the Koyna seismic zone, Western India. J Geol Soc India 81:289–290
Roychoudhury SC, Deshpande SV (1982) Regional distribution of carbonate facies, Bombay offshore region, India. am assoc Pet Geol Bull 66:1483–1496
Sabale PD, Meshram Sa (2012) Effect of dyke structure on ground water in between Sangamner and Sinnar area: a case study of Bhokani Dyke. Int J Comput Eng Res 2:1130–1136
Sahu R, Kumar a, Subbarao KV et al (2003) Rb–Sr age and Sr Isotopic composition of alkaline dykes near Mumbai: further evidence for the Deccan Trap-Réunion plume connection. J Geol Soc India 62:641–646
Sandwell DT, Smith, WHF (2009) Global marine gravity from retracked Geosat and ERS-1 altimetry: Ridge Segmentation versus spreading rate. J Geophys Res Solid Earth 114: B01411
Sarma SVS, Patro BPK, Harinarayana T et al (2004) a magnetotelluric (MT) study across the Koyna seismic zone, Western India: evidence for block structure. Phys Earth Planet Inter 142:23–36
Saunders aD, Jones SM, Morgan la et al (2007) Regional uplift associated with continental large igneous provinces: the roles of mantle plumes and the lithosphere. Chem Geol 241:282–318
Schaefer CJ, Kattenhorn Sa (2004) Characterization and evolution of fractures in low volume pahoehoe lava flows, eastern Snake River Plain, Idaho. Geol Soc am Bull 116:322–336
Schöbel S, de Wall H, Ganerød M et al (2014) Magnetostratigraphy and 40ar-39ar geochronology of the Malwa Plateau region (northern Deccan Traps), central western India: Significance and correlation with the main Deccan large Igneous Province sequences. J asian Earth Sci (in press). http://dx.doi.org/10.1016/j.jseaes.2014.03.022
Sen S (2011) Petrography and structural deformation of deccan basalt in and around Powai, India. Unpublished M.Sc. thesis, Indian Institute of Technology Bombay, India
Sen G, Bizimis M, Das R et al (2009) Deccan plume, lithosphere rifting, and volcanism in Kutch, India. Earth Planet Sci lett 277:101–111
Seton M, Müller R, Zahirovic S et al (2012) Global continental and ocean basin reconstructions since 200 Ma. Earth Sci Rev 113:212–270
Shah J, Srivastava DC, Pandian M et al (2007) Mesoscale fractures as palaeostress indicators: a case study from Cauvery Basin. J Geol Soc India 70:571–584
Sheth H (1998) a reappraisal of the coastal Panvel flexure, Deccan Traps, as a listric-fault controlled reverse drag structure. Tectonophysics 294:143–149
Sheth HC (2000) The timing of crustal extension, diking, and eruption of the Deccan flood basalts. Int Geol Rev 42:1007–1016
Sheth HC (2005) From Deccan to Réunion: no trace of a mantle plume. In: Foulger GR, natland JH, Presnall DC et al (eds) Plates, plumes and paradigms. Spec Pap Geol Soc am 388, pp 477–501
Sheth HC (2007) Plume-related regional prevolcanic uplift in the Deccan traps: absence of evidence, evidence of absence. Geol Soc am Spec Pap 430:785–813
Sheth HC, Pande K (2014) Geological and 40ar/39ar age constraints on late-stage Deccan rhyolitic volcanism, inter-volcanic sedimentation, and the Panvel flexure from the Dongri area, Mumbai. J asian Earth Sci 84:167–175
Sheth HC, Pande K, Bhutani R (2001a) ^{40}ar- ^{39}ar ages of Bombay trachytes: evidence for a Palaeocene phase of Deccan volcanism. Geophys Res lett 28:3513–3516
Sheth HC, Pande K, Bhutani R (2001b) ^{40}ar/ ^{39}ar age of a national geological monument: the Gilbert Hill basalt, Deccan Traps, Bombay. Curr Sci 80:1437–1440
Simpson C, Schmid SM (1983) an evaluation of criteria to deduce the sense of movement in sheared rocks. Geol Soc am Bull 94:1281–1288
Sippel J (2009) The Paleostress History of the Central European Basin System. Ph. D. thesis. Scientific Technical Report STR09/06, Dissertation zur Erlangung des akademischen Grades doctor rerum naturalium (Dr. rer. nat.) im Fachbereich Geowissenschaften an der Freien Universität Berlin
Sippel J, Saintot a, Heeremans M et al (2010) Paleostress field reconstruction in the Oslo region. Mar Pet Geol 27:682–708
Smith MR, Crespi JM, Steinen RP (2012) Paleostress analysis of post-alleghanian brittle faults from an exposure in the Putnam-nashoba Terrane, eastern Connecticut. Paper no. 40-10,

northeastern Section—47 annual Meeting abstracts. https://gsa.confex.com/gsa/2012nE/finalprogram/abstract_200128.htm. accessed on 30 nov 2013
Spencer JE (1984) Role of tectonic denudation in warping and uplift of low-angle normal faults. Geology 12:95–98
Srivastava DC, lisle RJ, Vandycke S (1995) Shear zones as a new type of palaeostress indicator. J Struct Geol 17:663–676
Stünitz H, Keulen n, Hirose T et al (2010) Grain size distribution and microstructures of experimentally sheared granitoid gouge at coseismic slip rates—criteria to distinguish seismic and aseismic faults? J Struct Geol 32:59–69
Subrahmanya KR (2001) arabian Sea—the prime witness to the Drama of India–Madagascar–Seychelles separation. Gondwana Res 4:792–793
Subrahmanyam C, Chand S (2006) Evolution of the passive continental margins of India—a geophysical appraisal. Gondwana Res 10:167–178
Talwani M, Reif C (1998) laxmi Ridge—a continental sliver in the arabian Sea. Mar Geophys Res 20:259–271
Tewari HC (2008) Deep seismic imaging of Indian continental crust and lithosphere. In: Subbarao KV, Sukeshwala Rn (eds) Deccan volcanism and related basalt provinces in other parts of the world. Geol Soc Ind Mem no. 3, Bangalore, pp 153–164
Tjia HD (1964) Slickenslides and Fault Movements. Geol Soc am Bull 75:683-686
Tjia HD (1967) Sense of fault displacements. Geol Mijnb 46:392–396
Todal a, Edholm O (1998) Continental margin off western India and Deccan large igneous province. Mar Geophys Res 20:273–291
Twiss RJ, Unruh JR (1998) analysis of fault slip inversions: do they constrain stress or strain rate? J Geophys Res Solid Earth 103:2205–12222
Vaidhyanadhan R, Ramakrishnan M (2008) Geology of India, vol 2. Geological Society of India, Bangalore, pp 733–784
Valdiya KS (2010) The making of India: geodynamic evolution. Macmillan, new Delhi, p 816
Valdiya KS (2011) Some burning questions remaining unanswered. J Geol Soc India 78:299–320
van Gent H, Back S, Urai Jl et al (2010) Small-scale faulting in the upper Cretaceous of the Groningen block (The netherlands): 3D seismic interpretation, fault plane analysis and regional paleostress. J Struct Geol 32:537–553
van Hinsbergen DJ, Steinberger B, Doubrovine PV et al (2011) acceleration and deceleration of India–asia convergence since the Cretaceous: roles of mantle plumes and continental collision. J Geophys Res Solid Earth 116:B6
Vandamme D, Courtillot V, Besse J et al (1991) Paleomagnetism and age determinations of the Deccan traps (India): results of a nagpur–Bombay traverse and review of earlier work. Rev Geophys 29:159–190
Vanderkluysen l, Mahoney J, Hooper P (2004) Implications for the emplacement of the Deccan Traps (India) from isotopic and elemental signatures of dikes. a GU Fall Meeting abstracts. http://adsabs.harvard.edu/abs/2004a GUFM.V51B0561V. accessed on 23 aug 2013
Vanderkluysen l, Mahoney JJ, Hooper PR et al (2011) The feeder system of the Deccan Traps (India): insights from dike geochemistry. J Petrol 52:315–343
Varun TR, Sainath BK, Ishwar nB (2009) Evaluating hydrocarbon potential of Deccan Trap (Basaltic Reservoirs) in padra field of Cambay Basin for its effective development through logging, geological and geophysical techniques. In: 2nd SPWla-India symposium, november
Verma nK, Kutty PSn, Sen G (2001) Imprints of strike slip movements in the Eocene–Miocene sequence of Western India Continental Shelf: implications for hydrocarbon exploration and production strategy. Geohorizons July issue:5–10
Viola G, Kounov a, andreoli Ma G et al (2012) Brittle tectonic evolution along the western margin of South africa: more than 500 Myr of continued reactivation. Tectonophysics 514–517:93–114
Waldron JWF, Roselli C, Johnston SK (2007) Transpressional structures on a late Palaeozoic intracontinental transform fault, Canadian appalachians. In: Cunningham WD, Mann P (eds) Tectonics of strike-slip restraining and releasing bends. Geol Soc lond Spec Publ 290, pp 367–385
Wallace RE (1951) Geometry of shearing stress and relation to faulting. J Geol 59:118–130
Watkeys MK (2002) Development of the lebombo rifted volcanic margin of southeast africa. In: Menzies Ma, Klemperer Sl, Ebinger, CJ et al (eds) Volcanic rifted margins. Geol Soc am Spec Pap 362, pp 27–46
Watts aB (2001) Isostasy and flexure of the lithosphere. Cambridge University Press, new York, p 458
Watts a, Cox K (1989) The Deccan Traps: an interpretation in terms of progressive lithospheric flexure in response to a migrating load. Earth Planet Sci lett 93:85–97
White R, McKenzie D (1989) Magmatism at rift zones: the generation of volcanic continental margins and flood basalts. J Geophys Res Solid Earth 94:7685–7729
White RS, McKenzie DP (1995) Mantle plumes and flood basalts. J Geophys Res Solid Earth 100:17543–17586
Whiteside P (1986) Discussion on 'large-scale toppling within a sackung type deformation at Ben attow, Scotland' by G. Holmes, JJ Jarvis. Q J Eng Geol Hydrogeol 19:439
Widdowson M (1997) Tertiary palaeosurfaces of the SW Deccan, Western India: implications for passive margin uplift. In: Widdowson M (ed) Palaeosurfaces: recognition, reconstruction and palaeoenvironmental interpretation. Geol Soc Spec Publ 120, pp 221–248
Widdowson M, Cox KG (1999) Uplift and erosional history of the Deccan Traps, India: evidence from laterites and drainage patterns of the Western Ghats and Konkan Coast. Earth Planet Sci lett 137:57–69
Widdowson M, Pringle M, Fernandez O (2000) a post K–T boundary (Early Palaeocene) age for Deccan-type feeder dykes, Goa, India. J Petrol 41:1177–1194
Xu S-S, nieto-Samaniego a, alaniz-Álvarez S (2012) Emplacement of pyroclastic dykes in Riedel shear fractures: an example from the Sierra de San Miguelito, central Mexico. J Volcanol Geotherm Res 250:1–8
Yamaji a (2000) The multiple inverse method: a new technique to separate stresses from heterogeneous fault–slip data. J Struct Geol 22:441–452
Yamaji a, Otsubo M, Sato K (2006) Paleostress analysis using the Hough transform for separating stresses from heterogeneous fault–slip data. J Struct Geol 28:980–990
Yatheesh V, Bhattacharya G, Dyment J (2009) Early oceanic opening off western India–Pakistan margin: the Gop basin revisited. Earth Planet Sci lett 284:399–408
Zachariáš J, Hübst Z (2012) Structural evolution of the Roudný gold deposit, Bohemian Massif: a combination of paleostress analysis and review of historical documents. J Geosci 57:87–103
Žalohar J (2009) T-TECTO 3.0 Professional. Integrated software for structural analysis of fault-slip data. Department of Geology, SI-1000 ljubljana, Slovenia. http://www2.arnes.si/~jzaloh/t-tecto_homepage.htm. accessed on 23 aug 2013
Žalohar J, Vrabec M (2007) Paleostress analysis of heterogeneous fault-slip data: the Gauss method. J Struct Geol 29:1798–1810